

ULTRASONIC COUPLANTS AT ELEVATED TEMPERATURES

By

Amala Kishore Mamilla

B.E. Andhra University (India) 2000

A THESIS

Submitted in Partial Fulfillment of the

Requirements for the Degree of

Master of Science

(in Mechanical Engineering)

The Graduate School

The University of Maine

August, 2004

Advisory Committee:

Michael Peterson, Associate Professor of Mechanical Engineering, Advisor

Donald Grant, R.C. Hill Professor and Chairman of Mechanical Engineering

Eric N. Landis, Associate Professor of Civil Engineering

ULTRASONIC COUPLANTS AT ELEVATED TEMPERATURES

By Amala Kishore Mamilla

Thesis Advisor: Dr. Michael Peterson

An Abstract of the Thesis Presented
in Partial Fulfillment of the Requirements for the
Degree of Master of Science
(in Mechanical Engineering)
August, 2004

The efficient transfer of ultrasonic energy depends on the ability of the couplant to make good surface contact across boundaries such as those between the buffer rod and the test piece. For high temperature ultrasonic testing selecting a couplant is an important barrier issue in many testing configurations. Improved couplants will decrease the error in determination of the attenuation and modulus of elasticity at elevated temperatures. Several possible high temperature couplant materials are considered. The attenuation of ultrasound through the dry couplant materials is then measured at elevated temperatures and appropriate testing is performed. It is expected that one of these materials will be used which softens near the testing temperatures of interest. This will result in improved ultrasonic coupling. It was found that the most effective couplants tested were aluminum and gold. For the temperatures over a range from 20 to 600°C, aluminum appears to be good couplant and gold over a range from 20 to 1100°C.

REFERENCES	60
APPENDIX A- THERMOCOUPLE TEMPERATURES (°C).....	62
APPENDIX B – ULTRASONIC SYSTEM SETTINGS	63
APPENDIX C- SOLUTION FOR THE SIMULTANEOUS EQUATIONS	64
APPENDIX D- SIGNAL PROCESSING MATLAB PROGRAMS	65
APPENDIX E- SAMPLES OF THROUGH AND PULSE-ECHO SIGNALS	77
APPENDIX F – DERIVATION OF THE RESPONSE OF THE COUPLANT MATERIAL BY	79
APPENDIX G- SAMPLE DATA SHEET FOR REFLECTION COEFFICIENT	80
APPENDIX H-RELATIVE ATTENUATION CURVES.....	84
BIOGRAPHY OF THE AUTHOR.....	89

LIST OF TABLES

Table A.1 Thermocouple temperature recordings with sapphire rod.....	62
Table A.2 Thermocouple temperature recordings with Fused Quartz rod.....	62
Table G.1 Sample data for reflection coefficient of brass.....	80
Table G.2 Sample data for reflection coefficient of aluminum.....	80
Table G.3 Sample data for reflection coefficient of copper.....	81
Table G.4 Sample data for reflection coefficient of gold.....	81
Table G.5 Sample data for reflection coefficient of PBI.....	82
Table G.6 Sample data for reflection coefficient of Pyrex.....	82
Table G.7 Sample data for reflection coefficient of silica glass.....	83

LIST OF FIGURES

Figure 2.1 Schematic representation of longitudinal ultrasonic waves	9
Figure 2.2 Schematic representation of transverse ultrasonic waves	10
Figure 2.3 Schematic diagram of the surface ultrasonic waves.....	11
Figure 3.1 Experimental Furnace setup along with endcap housing setup.....	23
Figure 3.2 Ultrasonic transducer setup with clamp attached to air cylinder rod	24
Figure 3.3 The preliminary temperature testing setup with thermocouples.	25
Figure 3.4 The four signals required for the signal processing.....	26
Figure 3.5 Schematic diagram of ultrasonic system setup.....	28
Figure 4.1 Samples of the couplants used for couplant study.....	32
Figure 5.1 A through transmission signal through an aluminum foil sample at 600°C.....	37
Figure 5.2 A pulse-echo signal through an aluminum foil sample at 600°C	37
Figure 5.3 Through transmission signal (X) before and after windowing.....	38
Figure 5.4 Pulse-echo signal (Y) before and after windowing	39
Figure 5.5(a) Schematic diagrams of the through transmission signals with spectrum response terms.....	42
Figure 5.5(b) Schematic diagrams of the through transmission signals with spectrum response terms.....	42
Figure 5.6 Attenuation curve of dry couplant aluminum sample at 200°C	45
Figure 6.1 Amplitude versus frequency curve of aluminum sample from 200-800°C	47
Figure 6.2 Amplitude versus frequency curve of brass sample from 200-1100°C.....	47

Figure 6.3 Amplitude versus frequency curve of copper sample from 200- 1100°C	48
Figure 6.4 Amplitude versus frequency curve of gold sample from 200-1100°C.....	48
Figure 6.5 Amplitude versus frequency curve of polybenzimidazole sample from 200-1100°C.....	49
Figure 6.6 Amplitude versus frequency curve of borosilicate glass sample from 200- 700°C	49
Figure 6.7 Amplitude versus frequency curve of silica glass sample from 200- 1100°C	50
Figure 6.8 Amplitude versus frequency curve of aluminum from 200-600°C with narrow Hanning window.....	51
Figure 6.9 Amplitude versus frequency curve of silica glass from 200-1100°C with narrow Hanning window.....	51
Figure 6.10 Amplitude versus frequency curve of gold from 200-1100°C with narrow Hanning window	52
Figure 6.11 Relative attenuation coefficient curve for aluminum from 200- 600°C	53
Figure 6.12 Relative attenuation coefficient curve for silica glass sample from 200-1100°C.....	53
Figure 6.13 Relative attenuation coefficient curve for gold sample from 200- 1100°C	54
Figure 6.14 Error bar showing range of data for three aluminum samples tested from 200-600°C	55

Figure 6.15 Error bar showing range of data for three silica glass samples tested from 200-1100°C	55
Figure 6.16 Error bar showing range of data for three gold samples tested from 200-1100°C.....	56
Figure 6.17 Average relative attenuation for different samples (0-600°C)	57
Figure 6.18 Average relative attenuation for different samples (0-1100°C)	57
Figure E.1. Through transmission signal for silica glass sample 1.....	77
Figure E.2 Pulse echo signal for silica glass sample 1.	78
Figure H.1 Relative attenuation coefficient curve for polybenzimidazole from 200- 1100°C.....	84
Figure H.2 Relative attenuation coefficient curve for silica glass2 from 200- 1100°C	84
Figure H.3 Relative attenuation coefficient curve for silica glass3 from 200- 1100°C	85
Figure H.4 Relative attenuation coefficient curve for gold 2 from 200-1100°C	85
Figure H.5 Relative attenuation coefficient curve for gold 3 from 200-1100°C.....	86
Figure H.6 Relative attenuation coefficient curve for copper from 200-1100°C	86
Figure H.7 Relative attenuation coefficient curve for brass at from 200-1100°C.....	87
Figure H.8 Relative attenuation coefficient curve for aluminum2 from 200- 600°C	87
Figure H.9 Relative attenuation coefficient curve for aluminum3 from 200- 600°C	88
Figure H.10 Relative attenuation coefficient curve for Pyrex from 200-600°C.....	88

Chapter 1

1. INTRODUCTION

1.1 Introduction

The two most important ultrasonic testing measurements are time delay and amplitude change of a wave propagating through a material. The ultrasonic velocity through a material is used to find the modulus of elasticity, if the density of the material is known. The change in the amplitude of the ultrasound after passing through the material provides additional information about the material such as porosity, damping and the presence of inhomogeneities.

Two configurations are typically used for ultrasonic testing, through transmission testing and reflection (pulse echo) testing. Using either configuration, ultrasonic measurement methods include measurement of amplitude changes and time delay changes of the ultrasound through the materials with respect to a reference material. Both methods can be used with intensity or amplitude measures to determine the attenuation of the ultrasound due to material. In this work we will consider primarily attenuation.

In order to propagate a wave in a solid material it is necessary to transmit an ultrasonic wave from a piezoelectric material into an unknown specimen. Due to the coupling variation at the interface between any two media the ultrasound passing can be attenuated and show significant variation, which causes difficulties in accurately measuring amplitude. This situation is particularly notable at high temperature. When ultrasonic velocity measurements in carbon-carbon composite samples are used to find the modulus of elasticity of the material, the ultrasonic

signal was highly attenuated due to coupling losses [Bunker, 2001]. Similar effects are seen when monitoring densification of ceramic materials [Peterson, 1994]. In both of these applications the amplitude of the ultrasound wave signal was significantly reduced that it was difficult to detect a transmitted ultrasonic signal. This loss of amplitude is due to coupling losses as well as material attenuation.

Materials exhibit attenuation that must be accounted for in any complete description of an ultrasonic measurement system [Schmerr, 1998]. Attenuation in materials is due to scattering and absorption of ultrasound that has passed through the medium. Attenuation due to scattering results from inhomogeneities like non-metallic inclusions and pores within the material or from the acoustic impedance changes at the interface between two materials. This acoustic impedance is the difference in density or sound velocity of the materials at an interface. Attenuation due to absorption results from the conversion of mechanical energy into heat during wave motion. The magnitude of the scattering loss, as well as the magnitude of absorption loss, constitutes attenuation [Krautkramer, 1975].

The attenuation of ultrasound due to material losses ranges from relatively low mean values in solid materials without fillers, such as acrylic resins (perplex), ethoxylene resin (cast resin), polystyrene, polyamide and Teflon to the very high values of attenuation which occur in the soft varieties of polyethylene (PE), polyvinylchloride (PVC) and polyisobutylene (Oppanol B) [Krautkramer, 1975]. Some other applications for attenuation measurement are detection of bubbles in the Teflon tube walls and evaluation of homogeneity of the thick plates of

polyethylene produced by thermoplastic pressing from granulates. Other non-destructive tests include laminations of the plastic material produced from sheets that can also be checked by measuring the attenuation of ultrasound. Ultrasonic measurements can also be used for quality tests on glass-fiber reinforced and carbon-fiber reinforced polymers and for determination of moisture content of plastics like polyamide. Solid-fuel rocket compounds and explosives can be tested for detection of voids and cracks by means of ultrasonic testing methods. These ultrasonic measurement methods include measurement of attenuation changes and acoustic velocity changes of ultrasound through the materials.

However, ultrasonic attenuation measurements are perhaps most familiar in biomedical fields. For instance, ultrasonic attenuation of excised tumor tissues can be measured in vitro and used to estimate the temperature increases due to ultrasonic absorption. Broadband ultrasound attenuation is an accepted indicator for assessment of osteoporosis. Ultrasonic imaging, an attenuation test, is most commonly associated with obstetrics.

Ultrasonic attenuation as the wave propagates through a material is always present to some degree. However reflections due to acoustic impedance mismatch and attenuation due to imperfect interfaces also occur. The later is the subject of this thesis. In particular, techniques to improve interface coupling at elevated temperature.

1.2 Attenuation of ultrasound at elevated temperatures

Currently, ultrasonic measurements at elevated temperatures have attracted some research attention. Measurements of the elastic moduli as a function of temperature for borosilicate glass and fused silica, elastically isotropic materials [Blodgett et. al., 1998], evaluation of dynamic properties of carbon-carbon composite at elevated temperatures [Bunker, 2002], nondestructive characterisation of carbon-carbon brake disks using ultrasonics [Joon-hyun lee et. al., 2001] and measurements of high temperature-elastic moduli and internal dilational and shear frictions of fused quartz [Fukuhara et. al., 1994]. The change in attenuation of ultrasound with the change in temperature in a material is one method of determining important material properties. Particularly in plastics, attenuation of ultrasound increases with increase in temperature [Krautkramer, 1975]. In the case of some metals attenuation also increases with the temperature. Steel has a maximum attenuation at its transition point from cubically body-centered to cubically face-centered iron (approx. 721°C) [Krautkramer, 1975]. However, any high temperature test is limited by the availability of couplants for high temperature testing.

The purpose of the ultrasonic couplant is to compensate for the imperfect contact between the surfaces of the media caused by the surface roughness. The couplant is generally used between the transducer and the surface of the work-piece to improve transmission of ultrasound. Smooth contact surfaces between the materials result in low attenuation due to the improved interface at the coupling surfaces. When surface roughness occurs, it is common to introduce a

viscous fluid to even out the imperfections. Water, oil, glycerin, grease, honey and petroleum jelly are the most commonly used couplants. Some plastics, rubbers and elastomers are also used as couplants. Dry elastomer couplants are used when the test pieces could be subject to contamination by the liquid couplants and where the application and removal of couplant liquids and gels is a problem.

High temperature testing is particularly difficult since couplants must be a viscous fluid at the temperature of interest. There is a need for the specialized couplants and specialized experimental techniques in order to obtain ultrasonic measurements at elevated temperatures. When working with hot work pieces, the difficulty of finding a suitable couplant increases with the temperature [Krautkramer, 1975].

1.3 Buffer rod technique

The basic problem in measuring the dynamic properties of materials using ultrasonic techniques at elevated temperatures is survival of the transducers that generate and detect the ultrasonic waves [Peterson, 1994]. The use of a buffer rod method is an efficient technique that can be used for thermally isolating the transducers from the hot test sample. If buffer rods, which serve as waveguides, are of sufficient length, the end remains cool enough so that the elevated temperature does not affect the piezoelectric transducer. The maximum temperature of the piezoelectric ultrasonic transducers must not exceed the Curie temperature. If the transducers are exposed to temperatures higher than the Curie temperatures of the material, the active piezoelectric element loses its properties

and becomes nonfunctional. A buffer rod technique was previously used to monitor the reaction bonding of silicon nitride [Peterson, 1994].

In this work, the buffer rods, made of a solid cylindrical fused quartz rod are used to guide the ultrasonic signal from a transducer, through a sample at elevated temperature and into the receiving transducer. The buffer rods have boundaries that have strong impedance mismatch to the surrounding gaseous medium. Waves impinging on these boundaries are reflected back in the structure and superpose to create a complex wave train. The structure is called a waveguide because of the conduction of the signal along the axis [Dual, 2001]. Appropriate signal processing techniques are used to remove the effects of the superposition of the waveguide modes and to calculate the attenuation of the ultrasonic signal passing through the sample.

1.4 Thesis statement

The efficient transfer of ultrasonic energy depends on the ability of the couplant to make good surface contact across boundaries such as those between the buffer rod and the test piece. For high temperature ultrasonic testing selecting a couplant is an important barrier issue in many testing configurations. Improved couplants will decrease the error in determination of the attenuation and modulus of elasticity at elevated temperatures. Several possible high temperature couplant materials are considered. The attenuation of ultrasound through the dry couplant materials is then measured at elevated temperatures and appropriate testing is performed. It is expected that one of these materials will be used which softens

near the testing temperatures of interest. This will result in improved ultrasonic coupling.

Chapter 2

2. THEORETICAL BACKGROUND

2.1 Elastic waves

Ultrasonic waves are mechanical or elastic waves that consist of oscillations or vibrations of the atomic or molecular particles of a substance about an equilibrium position of these particles. Ultrasonic waves have a greater frequency of oscillation than the highest frequency detectable by the human ear; 18-22 KHz. Elastic waves propagate in a medium with a restoring force. The elastic medium can be solid, liquid or gaseous.

2.1.1 Characteristics of waves

The ultrasonic wave like any other wave is the transfer of energy through the medium without the translocation of the medium. Wave length, cycle, frequency, amplitude are the important characteristics of the wave. The distance between two successive crests or troughs (compressions or rarefactions) is the wave length. The fall from a crest to a trough and subsequent rise to the next crest is a cycle. Frequency describes the number of cycles occurring in a given unit of time. The amplitude of a wave is the maximum displacement from the equilibrium.

2.1.2 Types of ultrasonic waves

Ultrasonic waves are classified as longitudinal waves, transverse waves, surface waves and guided waves depending on the particle displacement of the elastic medium.

2.1.2.1 Longitudinal waves.

Longitudinal waves travel through the medium as a series of alternate compressions and rarefactions. The particles transmitting the wave oscillate back and forth in the direction of travel of the waves. Since compression and dilation forces are active in these waves, they are also called compression waves. A schematic diagram of a longitudinal wave is shown in figure 2.1. In liquids and gases, the mean free paths of molecules at a pressure of 1 atm are so short that the longitudinal waves can be propagated simply by the elastic collision of one molecule with the next. These waves readily travel in elastic solid as well.

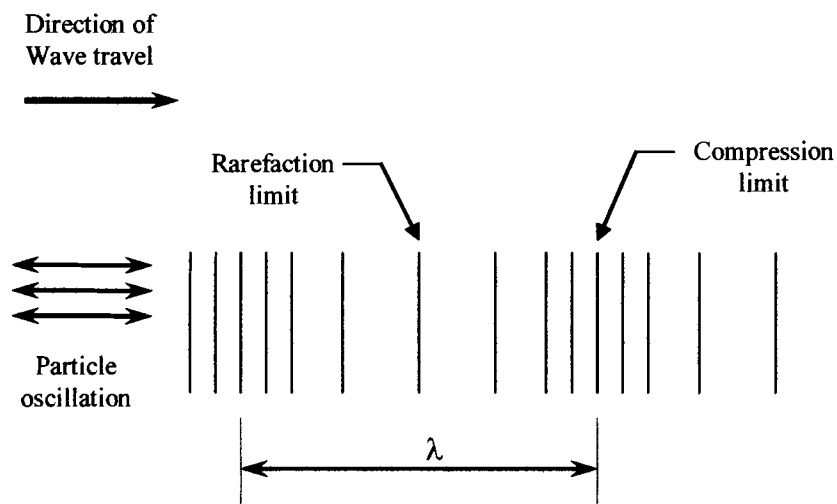


Figure 2.1 Schematic representation of longitudinal ultrasonic waves

2.1.2.2 Transverse waves.

In transverse waves the particles move up and down in a plane perpendicular to the direction of propagation. These waves are also known as shear waves since the restoring force is related to the shear modulus. A schematic diagram representing a transverse wave is shown in the figure 2.2. The transverse wave propagation requires the particles of the medium exhibit a strong force of attraction to its neighbors, so that as a particle moves up and down it pulls its neighbors with it with the same velocity as that of the transverse wave. Transverse waves propagate only through high viscosity liquids and solids. Due to small forces of attraction between the molecules, transverse waves do not transmit in gases.

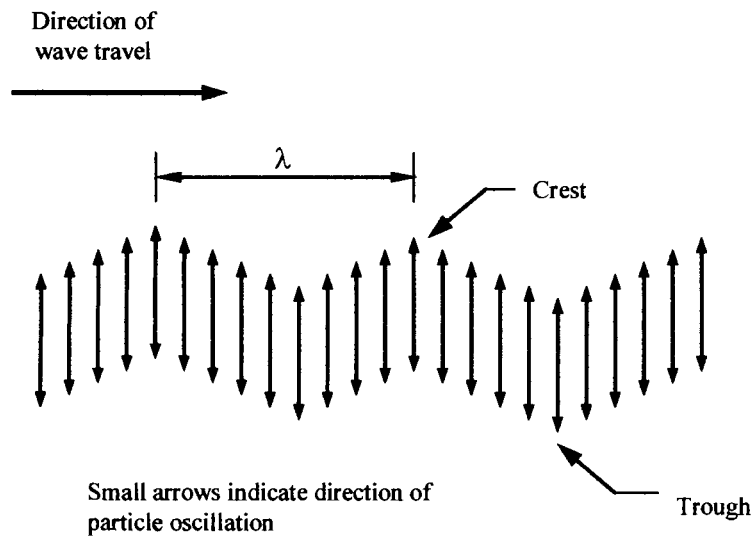


Figure 2.2 Schematic representation of transverse ultrasonic waves

2.1.2.3 Surface waves.

Surface or Rayleigh waves travel along the flat or large radius curved surface of a relatively thick solid material. Surface waves penetrate to a depth of approximately one wavelength. The propagation of this type of wave takes place at the interface bounded by a solid (strong elastic forces) on one side and a gas (negligible elastic forces) on the other side. The particle movement has an elliptical orbit. The schematic diagram of surface wave is as shown in the figure 2.3. Rayleigh waves generally follow contours. For instance, if all the edges of the cube are rounded sufficiently these waves will travel around the cube.

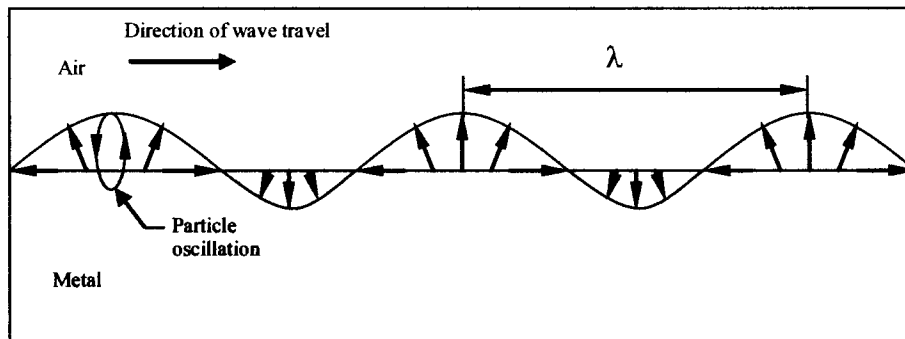


Figure 2.3 Schematic diagram of the surface ultrasonic waves

2.1.2.4 Guided waves.

Guided waves are waves with complex displacement patterns that propagate through the entire thickness of a material. In general the thickness is only a few wavelengths when these waves are generated. The guided waves can be generated as various modes with respect to frequency, thickness, and incident angle and they can propagate a large distance along the geometry of a structure.

The two geometries in which guided waves are commonly propagated are flat and circular cross section. Propagation of the Lamb waves in a flat cross section depends on the density, elastic properties and structure of the material, and is influenced by the frequency of the wave. In this work, guided waves through circular cross section having a traction free boundary are used. While an explanation of the guided waves is omitted, analysis of the data is performed for individual frequencies, so the complex signals are adequately addresses. Several references exist which support the approach. Prediction of longitudinal disturbances in a multimode cylindrical waveguide [Peterson, 1999], Mechanical Waveguides [Redwood, 1960] and Elastic waves in rods and clad rods [Thurston, 1978] are some of the references used.

2.1.3 Acoustic impedance

The transmission of ultrasonic wave from one medium to a second medium depends on the relative density and modulus of the two media. When a wave is incident on an interface between two materials, a portion of the incident energy is reflected back from the boundary while the remaining energy is transmitted into the second medium. The proportion reflected and transmitted is a function of acoustic impedance mismatch of the two materials. The acoustic impedance (Z) of a material is the product of density (ρ) and acoustic velocity (c) of that material.

If the impedances of the materials on either side of the interface differ greatly, there will be complete reflection. If the acoustic impedance is matched with two smooth surfaces, complete transmission of the wave occurs or perfect

coupling. Smooth surfaces which give perfect acoustic coupling allows the impedance mismatch to be the single factor that determines the transmitted and reflected wave. In this discussion, a homogeneous, isotropic elastic material is assumed. The acoustic impedance effects at a solid interface should not be confused with damping for a visco-elastic material or with losses due to scattering from material inhomogeneties.

2.2 Reflection and transmission (Normal incidence)

When a plane harmonic wave travels through the one medium, and strikes an interface at normal incidence, a part of this incident wave is reflected to the medium and the remaining part is transmitted to the second medium. Consider the reflected wave to be traveling in the negative x-direction and the transmitted wave to be traveling in the positive x-direction, the incident, reflected and transmitted waves can be written as [Schmerr, 1998]:

$$\begin{aligned}
 p_{inc} &= P_i \exp(ik_1x - i\omega t) \\
 p_{reflt} &= P_r \exp(-ik_1x - i\omega t) \\
 p_{trans} &= P_t \exp(ik_2x - i\omega t)
 \end{aligned}
 \tag{2.1}$$

where, P_i , P_r , and P_t are the pressure amplitudes of incident, reflected and transmitted waves. It is assumed that the amplitudes P_r , and P_t are unknown.

2.2.1 Reflection and transmission coefficients

At the interface, $x=0$, both pressure or stress and the normal component of the velocity must be continuous, so that

$$P_{inc} + P_{reflt} = P_{trans} \quad (2.2)$$

$$\frac{1}{i\omega\rho_1} \frac{\partial p_{inc}}{\partial x} + \frac{1}{i\omega\rho_1} \frac{\partial p_{reflt}}{\partial x} = \frac{1}{i\omega\rho_2} \frac{\partial p_{trans}}{\partial x} \quad (2.3)$$

Where ρ_1 and ρ_2 are the densities and c_1 and c_2 are the wave speeds of the two media respectively [Schmerr, 1998].

In terms of the amplitudes:

$$P_i + P_r = P_t \quad (2.4)$$

$$\left(\frac{ik_1}{\rho_1}\right)P_i - \left(\frac{ik_1}{\rho_1}\right)P_r = \left(\frac{ik_2}{\rho_2}\right)P_t \quad (2.5)$$

$$\text{when } k_1 = \frac{\omega}{c_1} \text{ and } k_2 = \frac{\omega}{c_2}$$

By solving the above two equations simultaneously as shown in the appendix, the ratios are found:

$$\frac{P_t}{P_i} = T_p = \frac{2\rho_2c_2}{\rho_1c_1 + \rho_2c_2} \quad (2.6)$$

$$\frac{P_r}{P_i} = R_p = \frac{\rho_2c_2 - \rho_1c_1}{\rho_2c_2 + \rho_1c_1} \quad (2.7)$$

where T_p and R_p are referred to as the transmission and reflection coefficients, respectively.

2.2.2 Reflection and transmission coefficients in terms of acoustic impedances

Normally in equation 2.6 and 2.7 the material properties are used as product of density and wave speed. For the first medium, $Z_1 = \rho_1c_1$ is the acoustic

impedance and similarly for the second medium the acoustic impedance is $Z_2 = \rho_2 c_2$.

In terms of acoustic impedance the reflection and transmission coefficients are given as [Schmerr, 1998]:

$$T_p = \frac{2Z_2}{Z_1 + Z_2} \quad (2.8)$$

$$R_p = \frac{Z_2 - Z_1}{Z_1 + Z_2} \quad (2.9)$$

This relationship assumes perfect contact and is an upper limit for transmitted energy. Any deviation from perfect contact further reduces the transmitted energy.

2.3 Coupling Methods

As previously mentioned, coupling of solids having a fine-machined surface finish with high pressures is one coupling technique. This brings the solids into intimate contact and can be used to overcome the gap impedance [Lynnworth, 1989]. Optically flat surfaces can be coupled by wringing them together. In the buffer rod system that is used in the present study, if the buffer rods are coupled without a couplant there is a huge attenuation in the signals recorded. The two buffer rods do not make intimate contact due to the surface roughness of the buffer rods, which causes this high attenuation to occur. In order to overcome the attenuation due to the surface roughness a couplant is introduced between the two buffer rods to create a smooth interface.

At elevated temperatures field installable couplants are much more useful. Teflon tape, gold foil and aluminum foil are some examples of solid couplants. For the current configuration pressure coupling is also useful at elevated temperatures on the order of 1000°C, since the fused quartz used as a buffer rod has a softening temperature at around 1200°C.

2.4 Different couplant types

Couplants can be of any form including, solid, liquid and gaseous. Solid couplants are further categorized as bonded or unbonded types. Bonded couplants include welded, brazed, soldered and adhesive bonded interfaces. Glass and wax may be bonded or unbonded. Couplants such as powders, metal foils, Teflon tape, rubber, grease, flux or other buffer that melts on contacting with the hot test sample are examples of couplants that do not bond. Other unbonded couplants include water, oil and glycol that are examples of liquid couplants with low viscosity. Gas and air are also used as couplants at very high pressures or with specially designed transducers.

Chapter 3

3. EXPERIMENTAL SYSTEM

In order to compare couplants at high temperatures a configuration was developed using an existing test apparatus. This system uses buffer rods to allow room temperature ultrasonic transducers to be used, without damaging the elements. Coupling was investigated between the two buffer rods used to isolate the transducers. This configuration eliminates the impedance mismatch at the interface so that only the effect of coupling is measured.

3.1 Furnace setup

The experiments for the attenuation study of couplants at high temperatures are conducted in a conventional tube type furnace. It is a three-zone furnace (Lindberg Model 55346, Watertown, WI) that has three individual embedded alloy heating elements (type LGO) capable of operating temperatures up to 1100°C. The heating elements surround a mullite tube 990.6 mm long and 40 mm outer and 32 mm inner diameters. This mullite tube runs horizontally through the furnace extending out on either side allowing the furnace to be sealed to control the atmosphere.

3.2 Waveguides

Waveguides were used in these applications to propagate the ultrasonic wave from a piezoelectric transducer into the high temperature controlled atmosphere furnace. The waveguide prevents the piezoelement from reaching the

Curie temperature. The waveguides must be sufficiently long and a cooling system is used to limit the maximum temperature of the transducer.

When selecting materials for the waveguides, material damping that will attenuate the wave as well as changes in modulus and damping must be considered. The waveguide must also be strong enough and sufficiently creep resistant to support its weight at temperature. The waveguides support their own weight, when cantilevered in the furnace, as well as a small compressive load when pressed against the sample while at high temperatures. Finally, thermal shock resistance must be adequate. The waveguide material selection was considered in previous work and quartz and sapphire were found to be the two best possible waveguide materials [Bunker, 2001].

Fused quartz rods, 10 mm in diameter, (Quartz Scientific, Inc., Fairport Harbor, OH) were chosen as the primary waveguide material for the dry couplant study since it has a relatively high compressive strength at elevated temperatures and small loss coefficient. Fused quartz is also inexpensive and could be easily cut with a tile saw to the desired lengths. Sapphire (Saphikon, Inc., Milford, NH) was the alternative material chosen for improved stability of the modulus with temperature.

The right side waveguide is slightly longer than the left side waveguide because of the right endcap that is one inch longer than the left. The left side waveguide is normally 585 mm (23 inches) long and the right side waveguide was 610 mm (24 inches) long. The waveguides are supported with an alumina fiber

tube whose outer diameter is equal to the diameter of the tube furnace. The waveguides fit inside the alumina tube are that supports the length of the rod.

3.3 Endcap setup

The endcaps on both ends of the furnace seal the mullite tube that extends outside the furnace. The end cap contains an air cylinder with 25 mm travel that retracts the waveguide from the sample and moves the waveguide into apply pressure between the sample and waveguides. The endcap has a sealed connector for the transducer cable and two other ports for the air cylinder hook ups. The air cylinder is fastened to a faceplate that has a hole at the center so that the air cylinder rod passes through it. The end of the air cylinder rod was bolted to a plate having three screws with springs around them. The springs are used to ensure a uniform force application on the waveguides so that they do not break. The springs will also accommodate moderate misalignment of the waveguide ends. The faceplate was connected to the transducer clamp with those three screws that can easily move in the plate allowing the springs around them to take any extra force generated by air cylinders due to transducer setup movement.

The faceplate is bolted to the endcap and then to the endcap housing foundation. The end cap housing foundation is a 165 mm long brass cylinder with 114.3 mm outer diameter and 63.5 mm inner diameters. To facilitate a tight sealing, an o-ring seal is held between the faceplate and endcap housing foundation. The o-ring sits in a 0.0101 m deep chamfer around the perimeter of the faceplate, which then forces a seal with the housing.

The transducer clamp holds the ultrasonic transducer and the waveguide. The waveguide is coupled to the transducer face with high temperature vacuum grease (Dow Corning, #976, Midland, MI) and kept in position with set screws. The waveguide end is cooled with a system, which clamps the waveguide but allows it to move in and out. Two rows of ball bearings contact the waveguide but allow the linear motion. The cylinder, which clamps the waveguide, is wound with copper tubing as a water cooling system, which circulates water from a reservoir to the brass cylindrical endcap housing. The cooling system transfers heat from the ball bearings. Figure 3.1 shows the system configuration.

3.4 Ultrasonic transducers

The experimental system used two transducers, which were supported, on either side of the furnace by the furnace endcaps as shown in Figures 3.1 and 3.2. One transducer was connected to a standard ultrasonic spike pulser (Panametrics model 5072PR, Waltham, MA) as a transmitting transducer. The second transducer was the receiving transducer, which was connected to an ultrasonic preamplifier (Panametrics 5660C, Waltham, MA). The pre-amp is used with the receiving transducer to amplify the signal received from the transducer for acquisition with a digital storage oscilloscope. An oscilloscope (Tektronix model TDS520A, Beaverton OR) was used with both transducer outputs for receiving the through transmission and the pulse echo signals. The transducers used were broadband nominal 1 MHz (central frequency) contact transducers (Panametrics model V103, Waltham, MA). Although the sample temperatures are very high, room temperature transducers are used in this work. Commercial high

temperature transducer with Curie temperatures are higher than the operating temperatures used are not available. The cooling system is sufficiently effective that room temperature transducers may be used. Avoiding use of high temperature transducers is desirable since high temperature transducers have lower efficiencies.

3.5 Testing of waveguides

The sample was positioned in the center of the furnace by the ends of the waveguides that extend into the furnace. The opposite ends of waveguides are outside the hot zone and are in contact with ultrasonic transducers. These cold ends of the waveguides are maintained below the Curie temperature of the piezoelectric material of the ultrasonic transducers by the cooling system. The temperature of the hot zone was varied from room temperature to 1100°C. To ensure that the system was operating correctly and to protect the transducers, the waveguide end surface temperatures were monitored during the testing.

The furnace has three independent heating elements, located near the center, with separate digital controllers. The controllers have two temperature readouts, one takes desired furnace temperature as input and the other one gives out the furnace temperature. The temperature in the furnace tube may not be equal to the controller readout temperature because of the mullite tube, alumina tube and spacing between the elements. However this difference is only on the order of 3 to 5 degrees at most as previously shown [Bunker, 2001].

3.5.1 Testing of sapphire waveguides

A preliminary test was performed on one of the sapphire waveguides to determine the temperatures at the end of the waveguides that contact the transducers. The temperature was compared at the transducer surface and the end of the waveguide in contact with the sample. A range of temperatures was used to determine the gradient in the furnace. This test was used to check the digital controllers as well as the thermal conductivity of the rod. The first test was performed on a small sapphire rod that is located on the left side of the furnace. The sapphire rod used was 230 mm (9 inches) long with two thermocouples (Omega, #XC-20-K, Stanford, CT) at the two ends. The thermocouples were attached to sapphire rods using two-part high temperature quick set epoxy (Manco Inc, #TM-51, Avon, OH). These thermocouples were then connected to a multi channel temperature-measuring device (Newport Electronics, Model INFBT10-0001-TC, Santa Ana, CA).

The test was conducted with the apparatus sealed from the atmosphere and the furnace heated to its maximum temperature of 1100°C. The temperature was slowly increased in increments of 25°C until the maximum temperature was attained. At each increment the furnace was left idle for 20 minutes in order to achieve a smooth increase in temperature. The smooth increase in temperature is to avoid the thermal shock due to an abrupt increase in temperatures. The temperatures at the end surfaces are noted for every 100°C decrement from the

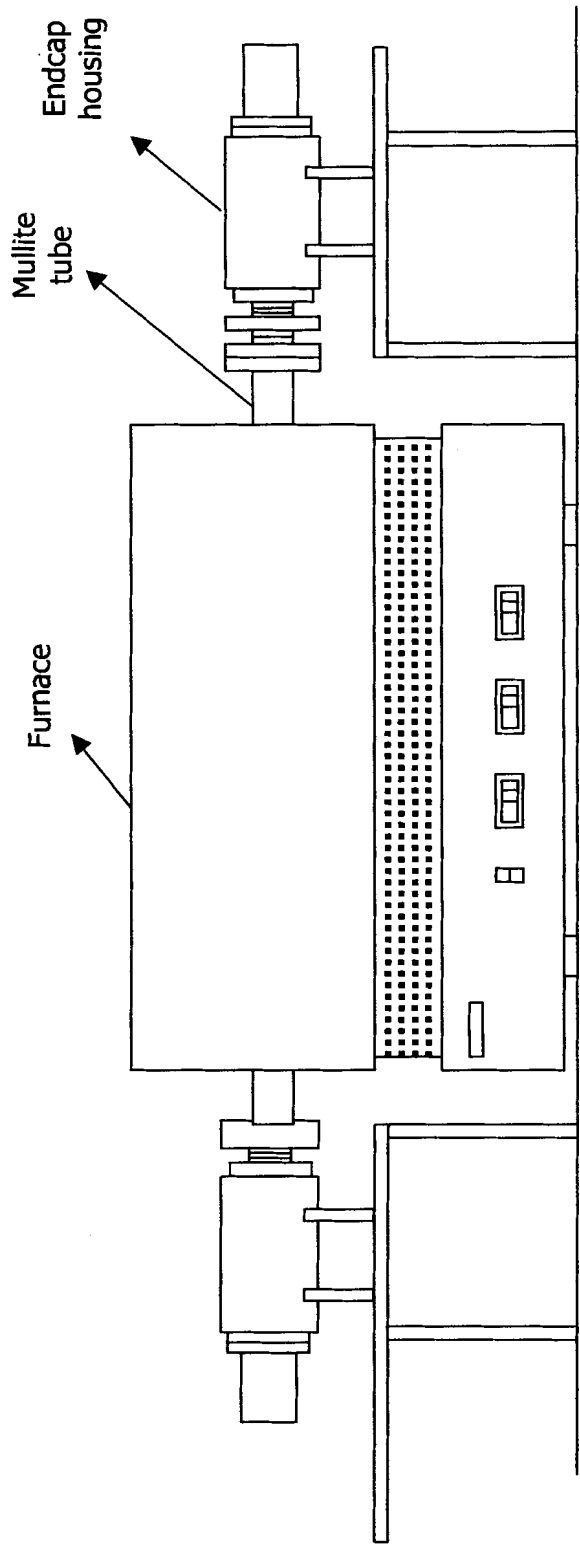


Figure 3.1 Experimental Furnace setup along with endcap housing setup

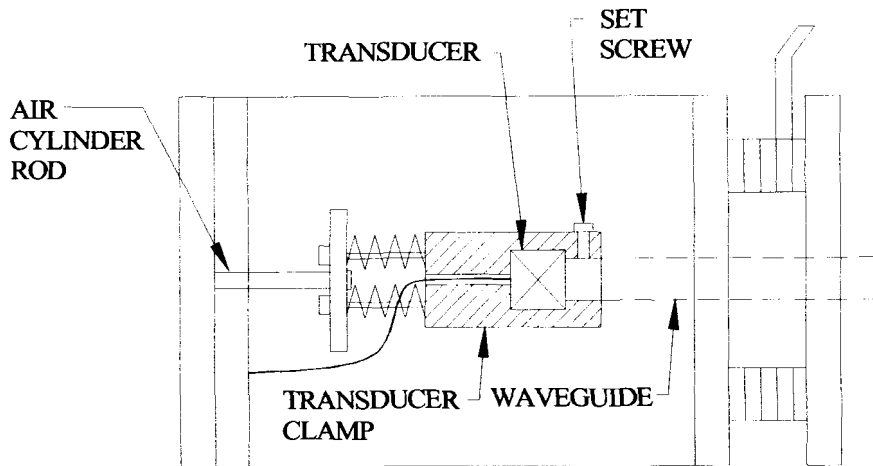


Figure 3.2 Ultrasonic transducer setup with clamp attached to air cylinder rod

maximum temperature. While cooling down the furnace, the temperature was decreased in the same fashion, in 25°C decrements. The measured temperatures at the end surfaces are given in tabular form in the appendix.

Experiments were also conducted using sapphire rods for an oxidation test on a carbon-carbon sample. Although the experiment was carried out using the same technique, with 25°C increments and 20 minute temperature soak, at 400°C the sapphire rods cracked. Thermal shock resistance of the sapphire was obviously a problem with the furnace.

3.5.2 Testing of fused quartz waveguides

Preliminary tests with fused quartz waveguides followed the same experimental procedure used with the sapphire waveguide test. For fused Quartz however the experimental the temperature was increased in 100°C increments.

Six K-type thermocouples were used (Omega, #XC-20-K, Stanford, CT). Two thermocouples were attached to the end surfaces. The remaining four thermocouples were attached to the quartz rod at every 10 cm distance. Figure 3.3 shows the preliminary temperature test with thermocouples arrangement. The results obtained from this test [Bunker, 2001] are shown in tabular form in appendix.

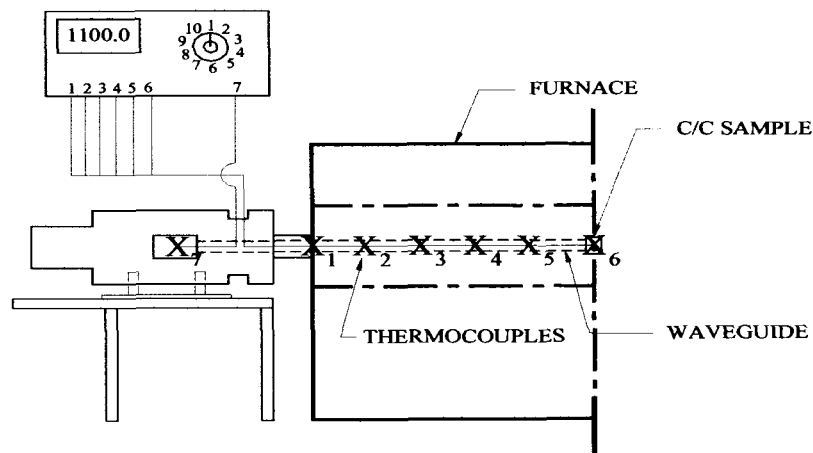


Figure 3.3 The preliminary temperature testing setup with thermocouples.

3.6 Data Acquisition

In order to perform the required signal processing for separation of the coupling response, two through transmission signals and two pulse echo signals, are needed for each data point. In order to acquire the signals the connectors for the ultrasonic signals must be switched on the furnace. A schematic diagram of the experimental set up for acquiring the four signals is as shown in figure 3.4. The signals and the notation used to describe them are included in the figure.

The signals noted as X and X' are through transmission signals, with Y and Y' as pulse-echo signals. The pulse-echo signals are obtained from the

reflection at the interface when the air cylinders are extended and the waveguides are in contact sample. The naming conventions for the signals along with some example signals recorded through the silica glass sample are shown in the appendix.

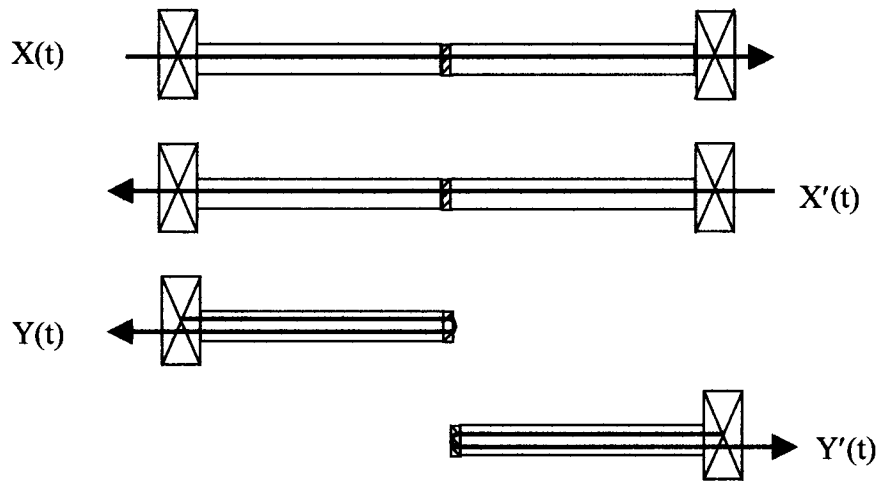


Figure 3.4 The four signals required for the signal processing.

When heating the furnace the waveguides are extended and are in contact. It is important to monitor the pressure in the cylinders when extending the waveguides. Allow initial pressure, 5-8 psi is used when extending the waveguides. The fused quartz waveguides have low fracture toughness and will shatter if they are extended too quickly allowing the faces of the waveguide to impact. Once the waveguides have been extended and are in contact, a higher pressure of 25 psi or 172.4 Kpa can be applied.

3.7 Data acquisition setup

For acquisition of a through transmission signal one of the transducers acts as transmitting transducer. The transmitting transducer is connected to an ultrasonic spike pulser (Panametrics Model 5072PR, Waltham, MA) that will excite the broadband ultrasonic signal.

To acquire the pulse echo signals each of the transducers is connected to the spike pulser. The spike pulser has a built in pre-amplifier for the received signal. The output of the spike pulser is input to the digital storage oscilloscope. Data acquisition is performed acquiring the signal using a GPIB interface from computer running a Lab View program. With the proper settings of the pulser, pre-amp and oscilloscope as shown in the appendix, the signal from the transducer has an acceptable signal to noise ratio. In addition the sampling rate of 250 Ms/sec, makes it possible to measure time delays with the precision of the sampling rate, or 4 nanoseconds in this case [Peterson, 1996]. The signal requires approximately 200 microseconds to propagate through the whole waveguide setup since the velocity of the ultrasonic wave is 3500 m/s. A time delay of 195 microseconds was used for triggering the oscilloscope. At the sampling rate used this delay allowed the complete signal, which propagated through the waveguide setup to be acquired.

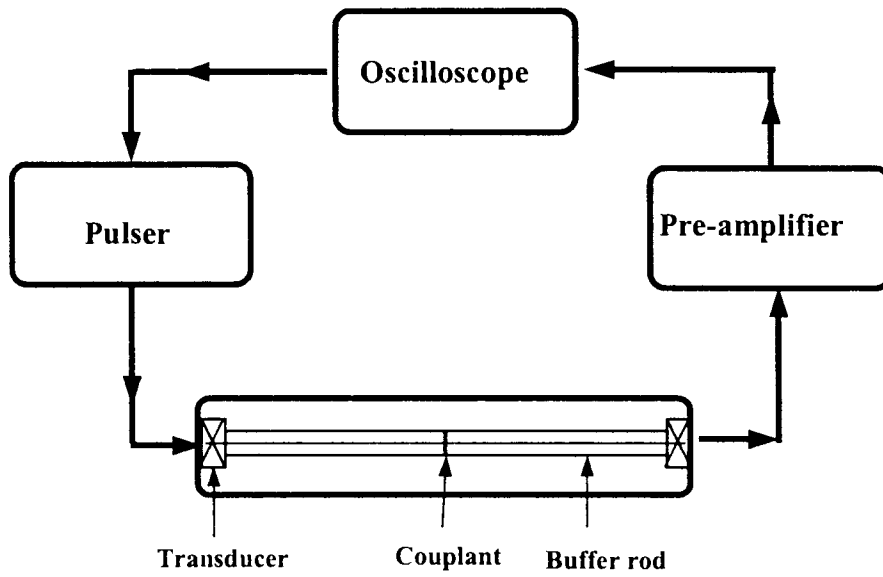


Figure 3.5 Schematic diagram of ultrasonic system setup

Chapter 4

4. EXPERIMENTAL PROCEDURES

The experimental procedures used for measuring the attenuation of ultrasound through dry couplant materials are discussed in this chapter. This chapter also includes couplant material selection, sample preparation, sample measurements, furnace preparation and atmosphere control procedures.

4.1 Couplant material selection

The candidate materials selected for this research are suitable for using as solid couplants in the evaluation of dynamic elastic properties and oxidation characteristics of carbon-carbon samples at elevated temperatures. High temperature couplant liquids and couplant gels, which are commercially available are not suitable for this purpose as the liquids and gels may contaminate the surface of the carbon-carbon sample and are not resistant to high operating temperatures. Materials that are solid at room temperature are best suited for this purpose. Though there are some plastics such as ABS (acrylonitrile-butadiene-styrene), PMMA (poly methyl methacrylate), delrin, nylon (black), polystyrene, PVC (poly vinyl chloride) and styrene butadiene and elastomers such as Dow silastic rubber, Ecogel 1265, polyurethane and pellathane thermoplastic urethane are already used as dry couplants in some applications. The usage of these materials is not suitable for the present application because of their low melting temperatures.

The melting point of the material plays an important role in the selection of couplants. As the material starts melting and forms liquid there is a possibility of the liquid material sticking to the surface of the test sample and contaminating the surface. The material must be solid or very viscous in the range of working temperatures. The ductility of the material also plays an important role in choosing the materials for couplant study as the dry couplant forms a thin layer filling the surface irregularities between the waveguide and the sample.

A review of physical properties such as melting point and ductility results in a number of dry couplants for evaluation. Aluminum foil, brass foil, copper foil, gold foil, PBI (Polybenzimidazole) fabric, borosilicate glass (Pyrex) and high-temperature silica glass are all potentially suitable materials.

4.2 Sample preparation

A brief description of the dry couplants selected and sample preparation of these dry couplant materials is given in this section. The aluminum foil selected is hard-temper aluminum foil roll (9012 K11, McMaster-Carr, Dayton, NJ) of 15.25 m long, 152.4 mm wide and 0.0025 mm thick. The foil is Alloy 1100/1145 and has a smooth and wrinkle free finish. Melting range is 643.33°C to 657.22°C. The material meets the QQA1876 specification. The brass foil (90355 K622, McMaster-Carr, Dayton, NJ) used for the present study is made of Alloy 260. This half-hard tempered foil is the most ductile of any brass. It is a 12.2 m roll of 50.8 mm wide and 0.8128 mm thick. The melting point of this alloy is 925°C and meets ASTM B36. The copper foil (9053 K312, McMaster-Carr, Dayton, NJ) is soft-tempered commercial grade, Alloy 110. It is a 30.5 m long roll of 50.8 mm

width, and 0.0508 mm thickness. The melting temperature of this alloy is 1083°C. The gold foil (Mister Art, Houston, TX) used for the study is a 25 mm square, edible 24 carat gold. Samples of 1 cm diameter from each of the metal foils are cut for testing.

PBI (Polybenzimidazole) fabric (8780 K8, McMaster-Carr, Dayton, NJ) is a soft textured synthetic fabric. This fabric is a blend of Kevlar/Aramid with PBI (Polybenzimidazole). This combination of materials provides temperature resistance up to 500°C. This fabric is 45.72 m long, 1 m wide and 0.7620 mm thick. The fabric is cut to 2 cm square samples. Borosilicate glass (8477 K11, McMaster-Carr, Dayton, NJ), also known as Pyrex or schott glass has a low coefficient of thermal expansion. The samples are available in circular plates or discs of 25.4 mm diameter and 3.175 mm thickness. The melting point of borosilicate glass is 600°C. The Silica Glass (8483 K51, McMaster-Carr, Dayton, NJ) samples are also available in discs. The maximum intermittent use temperature of high temperature silica glass discs is 1200°C. These samples are 25.4 mm in diameter and 3.175 mm in thickness. The density of each of the samples is given in tabular form in the appendix. Each of these candidate materials is suitable for use as couplants in the high temperature furnace.

4.3 Furnace preparation and procedures

The furnace preparation and procedures section describes all the steps involved in the assembly of the experimental setup to take the data. The first step in the assembly was applying high temperature vacuum grease (Dow-Corning #976, Midland, MI) to the o-ring gaskets located between the endcap faceplate and the

endcap housing. The ultrasonic transducer was placed in the transducer housing clamp and secured tightly with three set screws. A small amount of high temperature vacuum grease was applied to one end of the waveguide and firmly pushed against the transducer face. The waveguide was held in position in the transducer housing clamp with another three set screws. The small amount of vacuum grease applied to the end of waveguide acts as couplant between the transducer and the waveguide. After the transducer and the waveguide have been assembled, the endcap containing the air cylinder was fastened to the endcap housing foundation by slowly pushing the transducer housing into the endcap housing foundation.

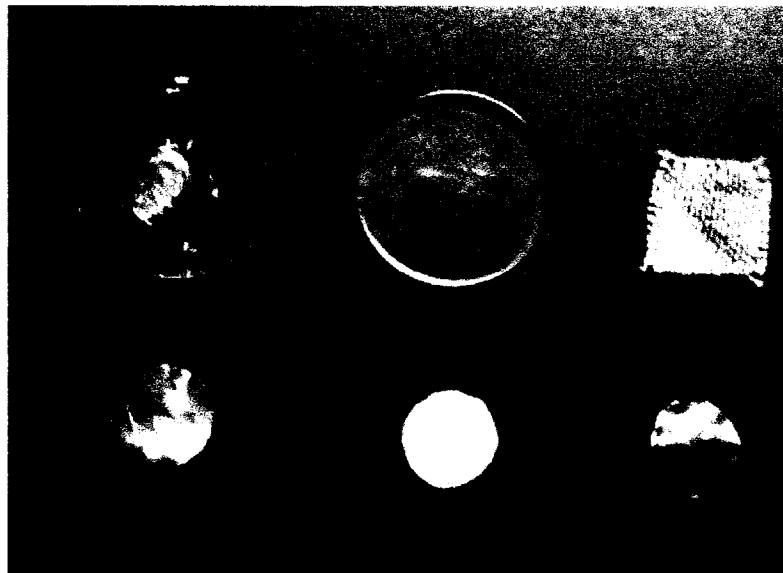


Figure 4.1 Samples of the couplants used for couplant study

The O-ring gaskets present between the endcap housing and the water cooling system and between the water cooling system and the sealing disks are also coated with vacuum grease. The rest of the endcap setup, including water

cooling system was fastened to the endcap housing foundation. Once the endcap setup was secured and sealed, the alumina tube was slid on the waveguide until it reached the endcap-housing end. This leaves a small portion of the waveguide uncovered. The uncovered end of the waveguide is cleaned and a small amount of couplant (UT-30, Sonotech, Inc., Bellingham, WA) was applied. The 1 cm diameter dry couplant samples were cut from the material rolls and were attached to the prepared end of the waveguide. The whole endcap setup is fixed to a Plexiglass plate, which was designed to slide on a carriage. The furnace endcap setup is slowly pushed into the furnace until the left side waveguide face with the sample attached to the face touches the other waveguide face. Slowly pushing the left waveguide's face against the right waveguide's face the furnace tube was allowed to sit in the groove formed by the endcap setup faceplates. These two faceplates force a high temperature Kalrez Perfluoroelastomer O-ring (McMaster-Carr, Dayton, NJ) to compress around the furnace tube and seal the furnace airtight. This seals the furnace so that data could be recorded using the experimental setup in a controlled atmosphere.

4.4 Inert atmosphere procedures

The experiments were carried out in a controlled atmosphere. The endcap setup has a small tube that extends from the interior of the experimental setup to tubing on exterior of the furnace. Fittings attached to the tubing were used to evacuate and backfill the furnace with a controlled atmosphere. To evacuate the furnace atmosphere, a medium vacuum pump (Marvac Scientific, Model #R-10,

Concord, CA) with a vacuum control valve was used. The tube furnace is pressurized to 100 Kpa or 14.5 psi with nitrogen. The furnace atmosphere is then evacuated with the vacuum pump and then backfilled with an inert gas. Testing is then performed with the furnace tube maintained at a slight positive pressure. Leaks do not introduce oxygen into the system. A flow meter is used to determine the extent of leakage and it is sealed if excessive. Nitrogen gas was used to fill the atmosphere and also supply the pressure to the air cylinders.

Chapter 5

5. SIGNAL PROCESSING

5.1 Introduction

Attenuation results from the absorption of energy by the medium between the two points and from the deflection of the energy from the propagation path of the ultrasound by reflection, refraction, diffraction and scattering [Cracknell, 1980]. The absorption of the ultrasound is dependent on the medium in which it propagates. The material damping reduces the magnitude of the wave and is useful in studying the physical properties of the medium. The absorbed ultrasound is converted to heat energy from the displacement of the particles. Reduction in the amplitude of the ultrasonic wave also results from scattering due to material inhomogeneties. The reduction in the intensity of the ultrasound wave through the medium due to scattering and damping is measured as attenuation. The dynamic material attenuation is in addition to the velocity of the ultrasonic wave.

The change in velocity of the wave in materials at elevated temperatures is caused by the changes in density and elastic modulus of the materials. When studying only the coupling layers, the velocity changes are quite small. Thus, the attenuation of the ultrasonic wave through the coupling interface was the primary concern of this work.

In order to measure the ultrasonic attenuation, appropriate signal processing is required. Signal processing allows the changes in the couplant to be separated from other effects. Signal processing of the data obtained from the

experimental setup involves mainly two primary steps, windowing and deconvolution of the signals.

5.2 Signal windowing

The first part of the signal must be separated to eliminate multiple reflections from within the buffer rods. The attenuation of the coupling materials with change in temperature is determined by deconvolution of the signals obtained after isolating the initial signal. The through transmission and pulse-echo signal through an aluminum foil sample before windowing are shown in the figure 5.1 and figure 5.2 respectively. A window function reduces the amplitude of the first and last part of the selected portion of the signal, which better maintains the characteristics of interest.

While windowing is required to eliminate multiple reflections of the ultrasonic signal, uncertainty in the location of the signal of interest results in a strong sensitivity to choice of windows. There are many different types of windowing functions. The window used in the current work is a Hanning window. The Hanning window cuts the time record smoothly, reducing the high frequency energy that is introduced, when the data is cut off. A Hanning window has the following form:

$$w(x) = \begin{cases} 0 & x < A \\ .5(1-\cos(2\pi x/B)) & A \leq x \leq B \\ 1 & B < x \leq (D-B) \\ .5(1-\cos(2\pi x/B)) & (D-B) < x \leq D \\ 0 & x > D \end{cases} \quad (5.1)$$

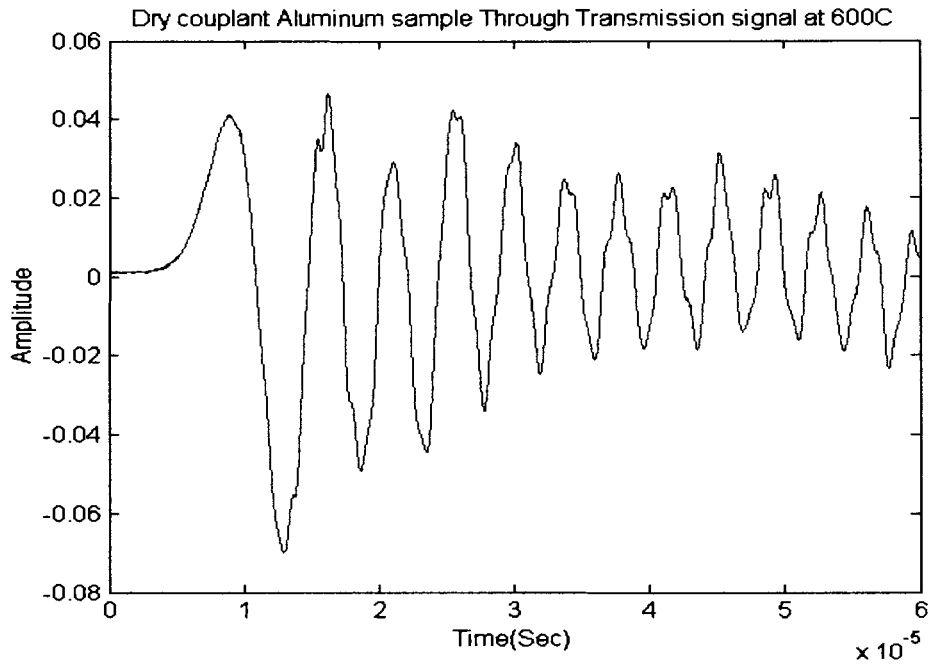


Figure 5.1 A through transmission signal through an aluminum foil sample at 600°C

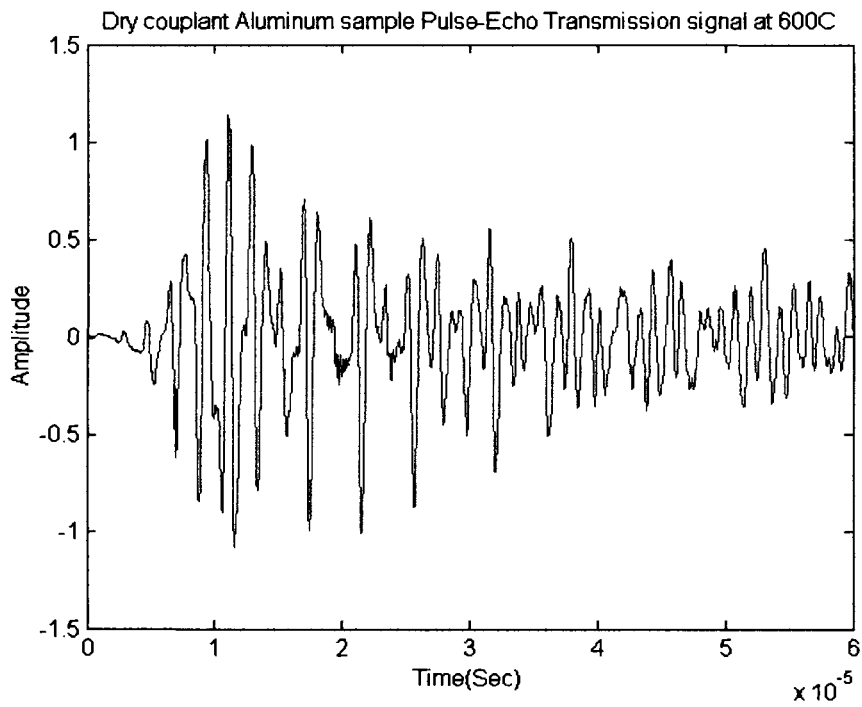


Figure 5.2 A pulse-echo signal through an aluminum foil sample at 600°C

The length of the Hanning window can be adjusted depending upon the length of the signal required. The length of the Hanning window is kept constant when windowing a set of signals. A Matlab program is written for the above window function. This program takes the number of data points before the start of the Hanning window, the width of the Hanning window, the number of data points in the Hanning window and the end of the Hanning window as input and outputs the required signal data for the deconvolution of the signal. The appendix shows the Matlab program that uses the Hanning window for selection of the appropriate ultrasonic signal.

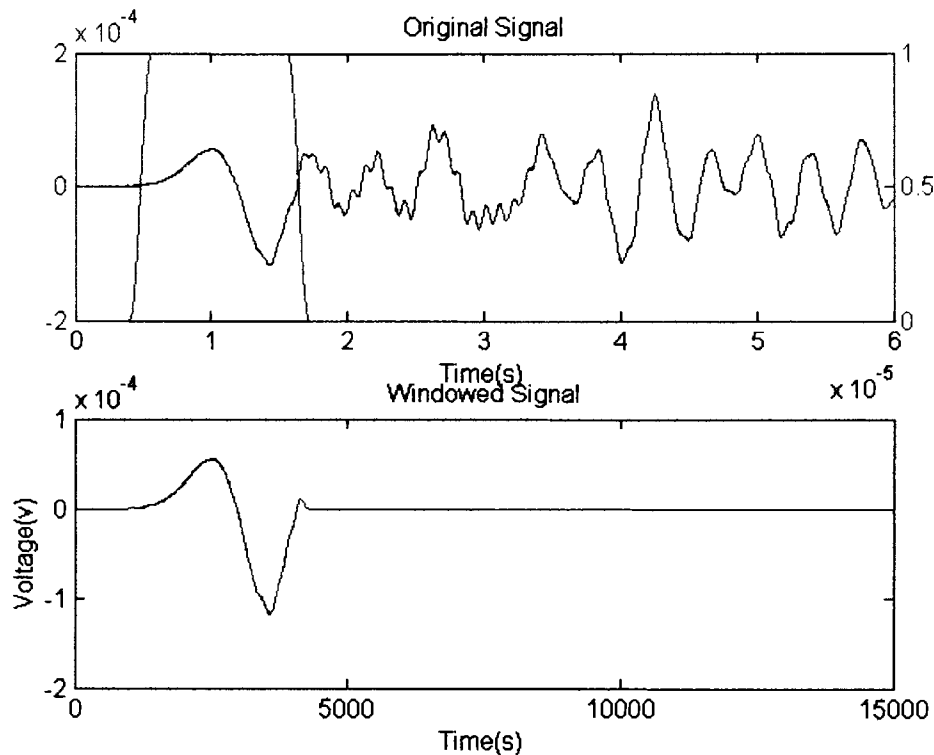


Figure 5.3 Through transmission signal (X) before and after windowing

The figure 5.3 shows the unwindowed and windowed through transmission signal. The upper trace of the figure 5.3 is an unwindowed signal

with the Hanning window superimposes as a second line. The lower trace of the figure 5.3 is windowed signal used for deconvolution of the signals from which is obtained the attenuation. The figure 5.4 is an unwindowed and windowed pulse-echo transmission signal. The lower trace of this figure is used in deconvolution of the signals.

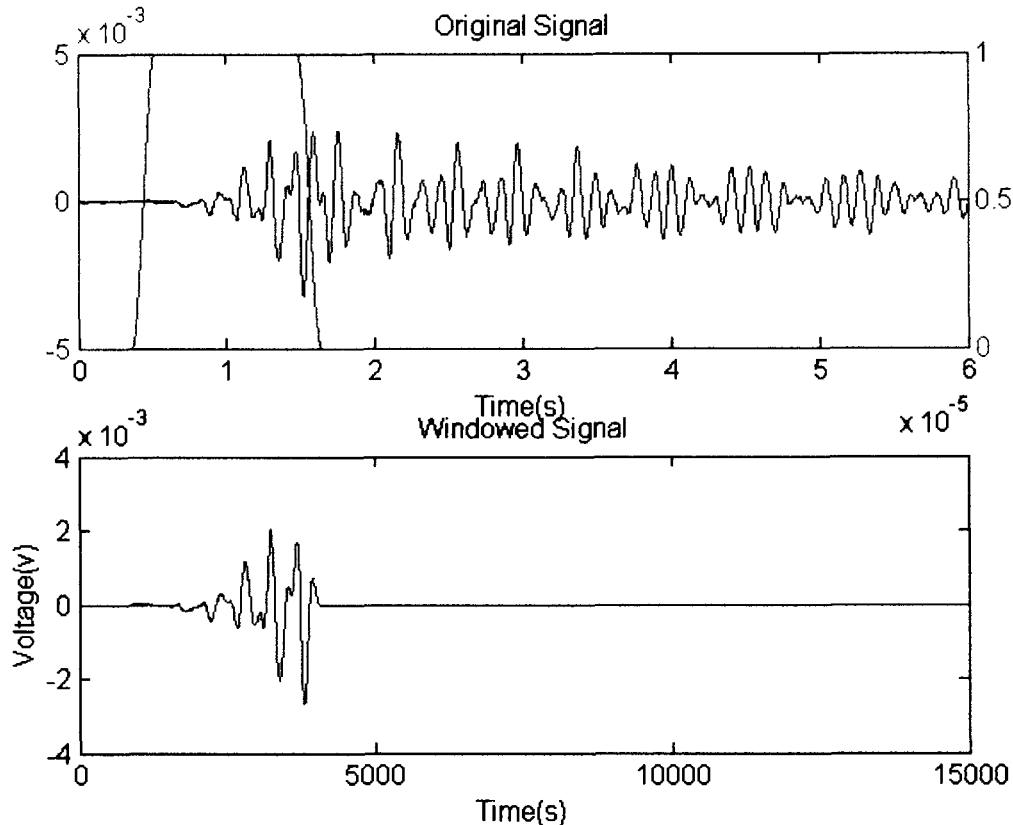


Figure 5.4 Pulse-echo signal (Y) before and after windowing

5.3 Deconvolution

The heating of the furnace brings change in the response of the transducer, response at the interface between the transducer and the waveguide, response of the waveguides and the response due to coupling. The response of the couplant with change in temperature is the subject of the present study of couplant

materials. The deconvolution of the signals separates the response of the couplant material from the changes that occur during heating from the responses of the unwanted signatures. The effects such as changes between the buffer rods and transducer coupling, the buffer rods and the sample high temperature coupling, wave speed or attenuation in buffer rods and changes in the response characteristics of the piezoelectric transducers are eliminated by deconvolution. A general understanding of the system is important since the form of deconvolution is developed by the arguments based on the physical system [Peterson, 1994]. The magnitude and phase of the spectrum of the four signals used are obtained using the discrete Fourier transfer (DFT) algorithm. The DFT of the signal was carried out by using a Matlab built in function $\text{fft}(x,n)$. If the length of X (when $X = \text{fft}(x,n)$) is less than n , X is padded with trailing zeros to length n . If the length of X is greater than n , the sequence X is truncated. When X is a matrix, the length of the columns is adjusted in the same manner.

$$X(k) = \sum_{j=1}^N x(j) \omega_N^{(j-1)(k-1)} \quad (5.2)$$

where

$$\omega_N = e^{(-2\pi i)/N}$$

The signals used are repeated where the end of the sequence is the beginning of the next repetition. Thus zero padding does provide additional information for a non-repeating signal. The discrete Fourier transform is performed on the signals that are obtained after applying the windowing function. The spectra obtained are designated $X(\omega)$, $X'(\omega)$, $Y(\omega)$ and $Y'(\omega)$. Each of the signals is comprised of the convolution (multiplication in the time domain) of the

contributing response functions for the signal. The form of the convolved signal in terms of the transfer function of the components is:

$$X(\omega) = A_{1t}(\omega)H_{1b}(\omega)H_b(\omega)H_c(\omega)H_b'(\omega)H_{1t}'(\omega)A_{2r}(\omega) \quad (5.2)$$

$$Y(\omega) = A_{1t}(\omega)H_{1b}(\omega)H_b(\omega)R_{bc}(\omega)H_b(\omega)H_{1t}'(\omega)A_{1r}(\omega) \quad (5.3)$$

$$X'(\omega) = A_{2t}(\omega)H_{1b}'(\omega)H_b'(\omega)H_c(\omega)H_b(\omega)H_{1t}'(\omega)A_{1r}(\omega) \quad (5.4)$$

$$Y'(\omega) = A_{2t}(\omega)H_{1b}'(\omega)H_b'(\omega)R_{bc}'(\omega)H_b'(\omega)H_{1t}'(\omega)A_{2r}(\omega) \quad (5.5)$$

Where:

$A_{nx}(\omega)$ = spectral response of transducer n in x = t, transmit or x = r, receive mode.

$H_{1b}(\omega)$ = spectral response from coupling between transducer 1 and buffer rod 1.

$H_b(\omega)$ = spectral response of buffer rod 1.

$R_{bc}(\omega)$ = spectral response of reflection from dry coupling between buffer rod 1 and sample.

$H'_{1b}(\omega)$ = spectral response from coupling between transducer 2 to buffer rod 2.

$H'_b(\omega)$ = spectral response of buffer rod 2.

$R'_{bc}(\omega)$ = spectral response of reflection from dry coupling between buffer rod 2 and sample.

$H_c(\omega)$ = spectral response of couplant layer, the objective of the study.

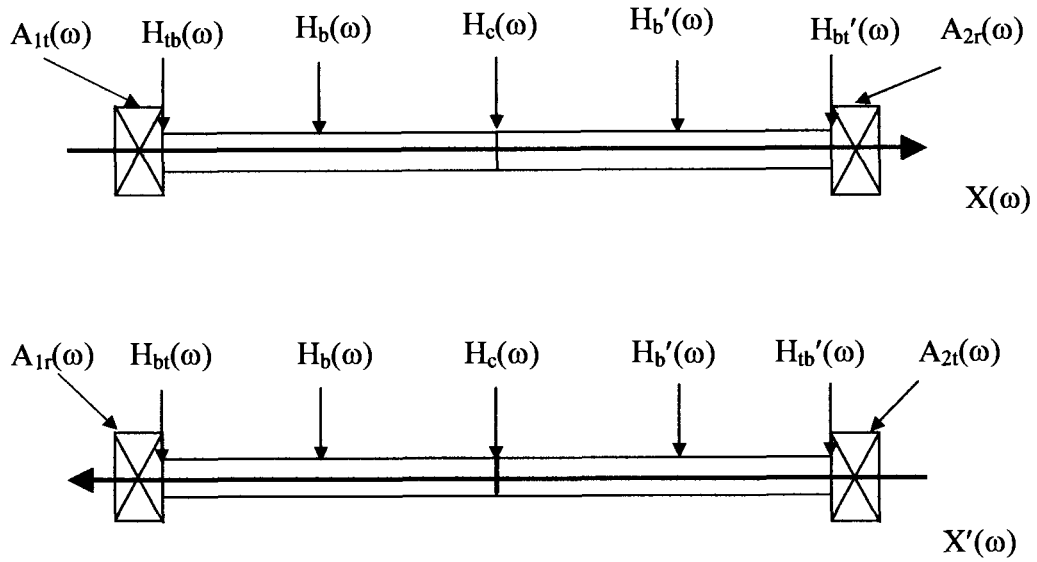


Figure 5.5(a) Schematic diagrams of the through transmission signals with spectrum response terms

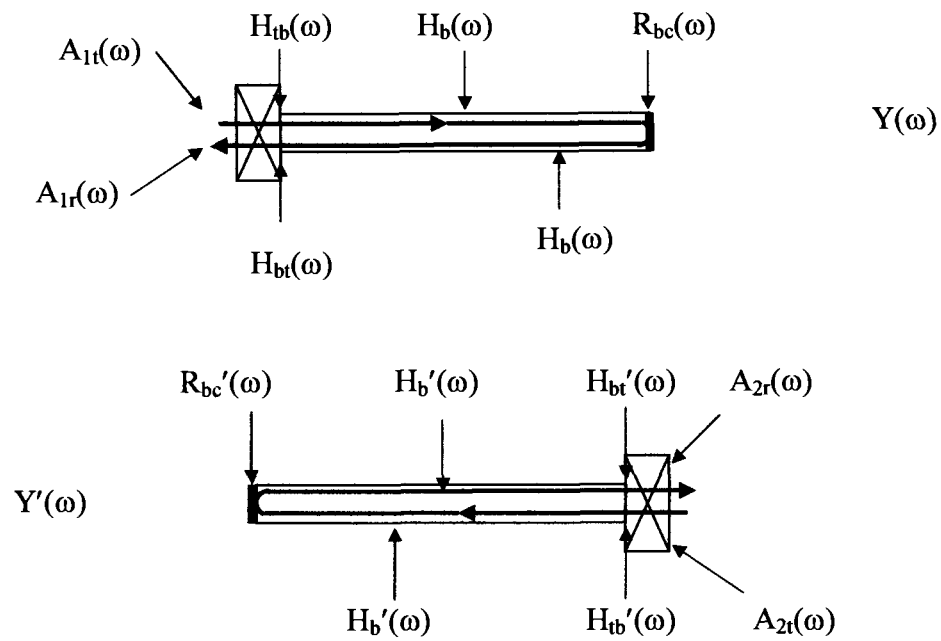


Figure 5.5(b) Schematic diagrams of the through transmission signals with spectrum response terms

A schematic diagram of the through transmission signals and pulse-echo signals with response terms labeled is shown in figure 5.5(a) and figure 5.5(b). The response of the couplant material is separated from the total response of the signal by deconvolution. The response of the dry couplant material, $H_c(\omega)$ is found from:

$$H_c(\omega) = \sqrt{(R_{bc})^2 \left(\frac{X(\omega)X'(\omega)}{Y(\omega)Y'(\omega)} \right)} \quad (5.6)$$

where:

$$R_{bc} = \frac{\Delta_2 - \Delta_1}{\Delta_1 + \Delta_2}$$

$$\Delta_2 = \frac{\rho_2}{\rho_1}, \quad \Delta_1 = \frac{c_1}{c_2}$$

The term $R_{bc}(\omega)$ is given by:

$$R_{bc} = \frac{\frac{\rho_2}{\rho_1} - \frac{c_1}{c_2}}{\frac{c_1}{c_2} + \frac{\rho_2}{\rho_1}}$$

where:

ρ_1 is the density of the buffer rod,

ρ_2 is the density of the dry couplant sample,

c_1 is the velocity of the ultrasonic wave at the required temperature in buffer rod,

c_2 is the velocity of the ultrasonic wave at the recording temperature of the dry coupled sample.

A derivation is included as an appendix. The deconvolution of the signal is performed without the use of a stabilizing term in the denominator. The stabilizing term in the denominator is often required in normal deconvolution because of instability in the numerical process of division by a small number. Typically the stability is implemented as a Weiner or pseudo-Weiner deconvolution [Karpur et. al., 1990]. In this case a term, on the order of 0.1% of the peak amplitude, was actually found to increase the instability of the calculations.

The changes in wave velocities as a function of temperature for fused quartz are noted [Fukuhara et. al., 1994]. In the calculation of R_{bc} at different temperatures, the change in velocity of the ultrasonic waves in the dry couplant material is not considered. This is reasonable since the thickness of the sample is very small for all materials except the glass. Properties such as density, wave speed in the buffer rods at different temperatures and wave velocity of the dry couplant material are given in a table in appendix. The calculated reflections at the buffer rod interface at different temperatures are also given in the same table.

Using the transmission response equation a Matlab program that gives the attenuation of the dry couplant material is shown in appendix. This program performs a DFT of the windowed signal and then deconvolves the signals to give the attenuation curve.

Relative attenuation of the couplant material is obtained by simply dividing, the magnitude of the response of the couplant with the magnitude of the response of the base case (with out any couplant sample). The magnitude of the

response of the base case is very high when compared to the response of the couplant material. So in obtaining the relative response of the couplant material, the response of the aluminum sample at room temperature is used instead of dry coupling. The attenuation curve for dry couplant aluminum sample at 200°C is as shown in figure 5.6. The simple division process in obtaining the relative attenuation is really a deconvolution carried out in frequency domain. Taking logarithm of the relative attenuation the relative attenuation coefficient α is attained. The Matlab program for finding a curve of the coefficient of relative attenuation versus frequency is given in the appendix.

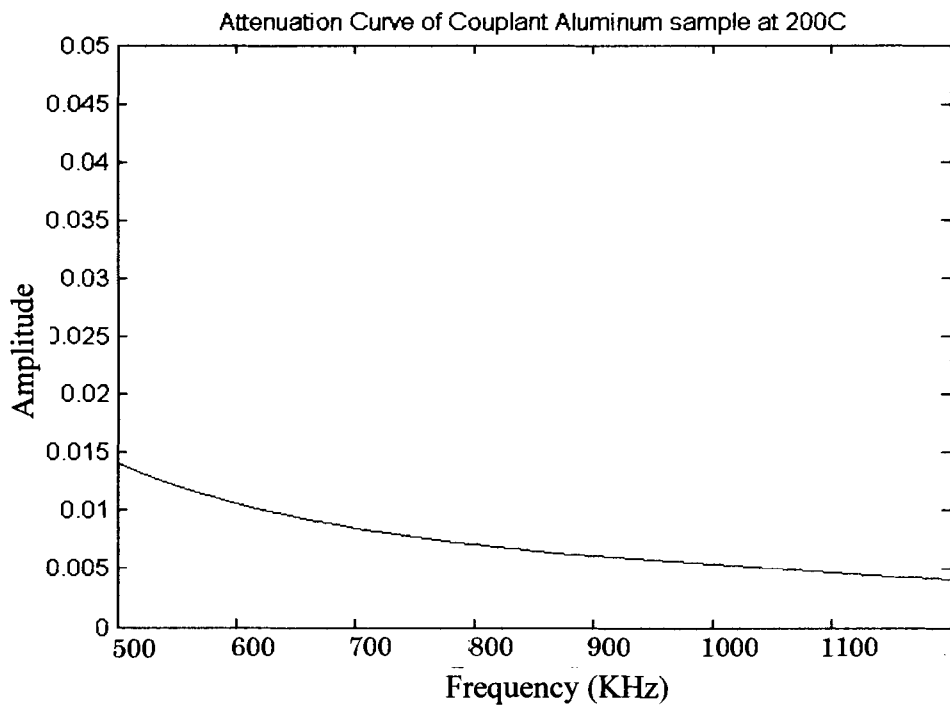


Figure 5.6 Attenuation curve of dry couplant aluminum sample at 200°C

Chapter 6

6. RESULTS

6.1 Introduction

The results section consists of the attenuation curves obtained for each of the dry couplant samples. These curves were obtained for temperatures that were below the melting or degradation temperature of the materials. While a number of samples were initially tested, a smaller number of samples that showed promise in the initial screening were further selected for study. The experiments at the elevated temperatures were repeated for the samples selected. Several candidate materials show reasonable repeatability for the attenuation values when compared to dry coupling.

6.2 Attenuation curves

The ultrasonic wave signals obtained from the experimental setup described previously for all of the samples are obtained and analysis of the signals obtained is carried out. The frequency versus attenuation plots obtained after deconvolution for different couplant samples at their appropriate temperatures are given in the figures 6.1 to 6.7.

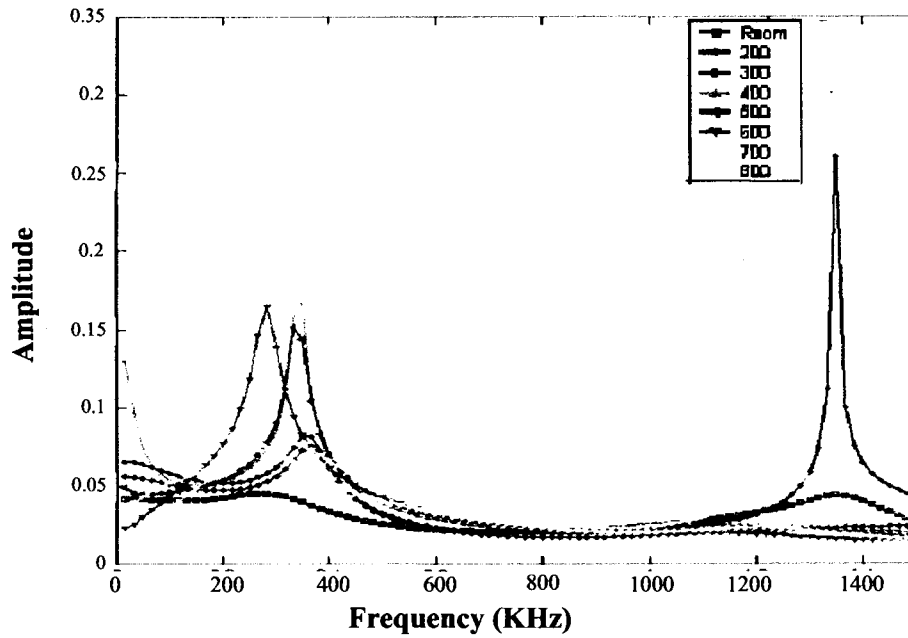


Figure 6.1 Amplitude versus frequency curve of aluminum sample from 200-800°C

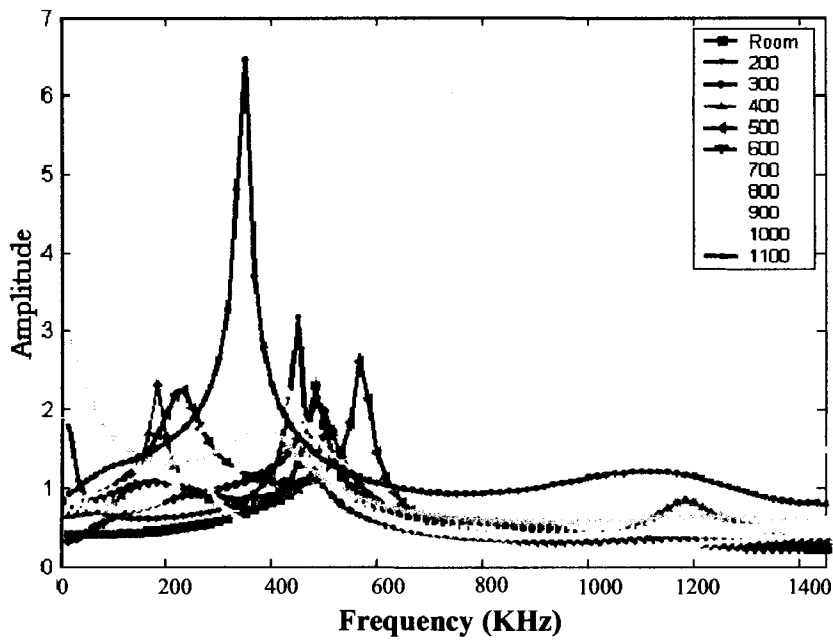


Figure 6.2 Amplitude versus frequency curve of brass sample from 200-1100°C

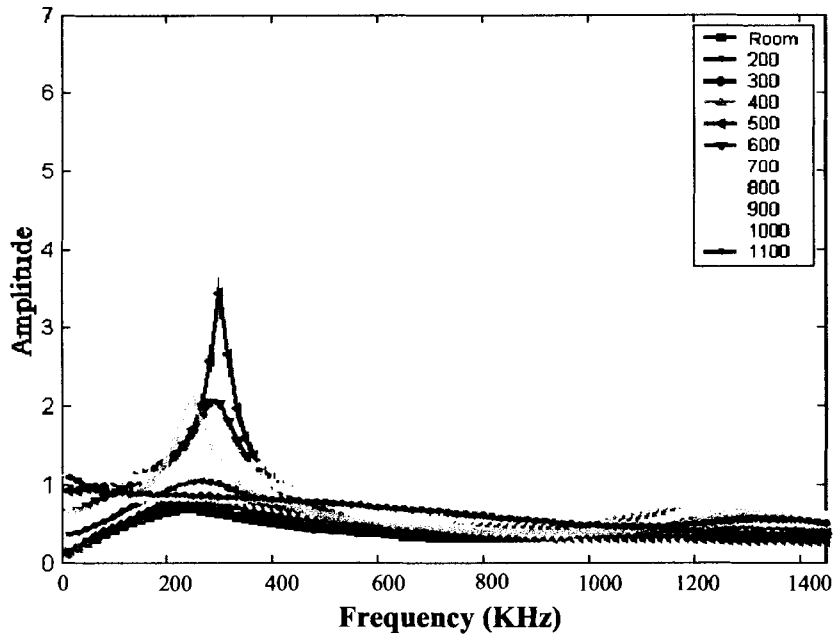


Figure 6.3 Amplitude versus frequency curve of copper sample from 200-1100°C

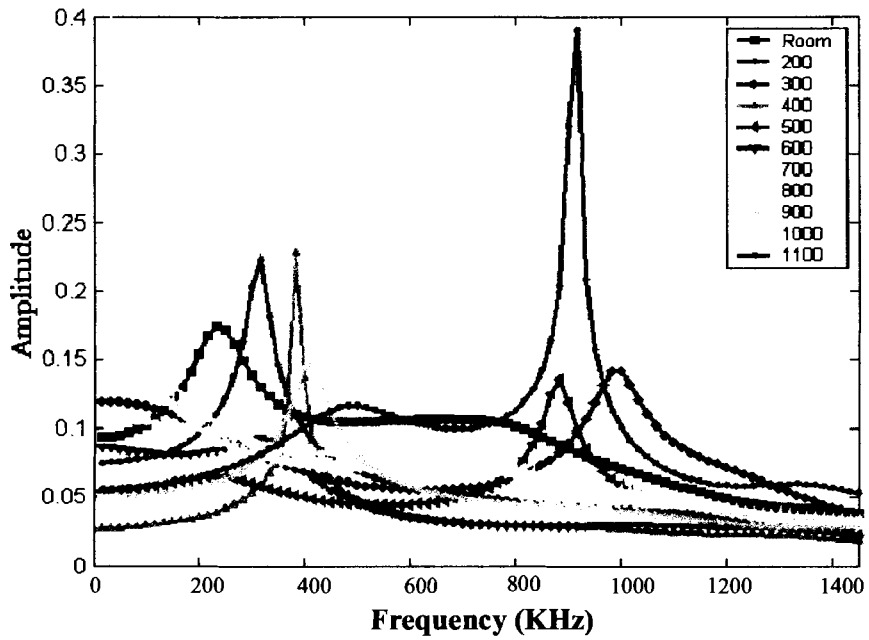


Figure 6.4 Amplitude versus frequency curve of gold sample from 200-1100°C

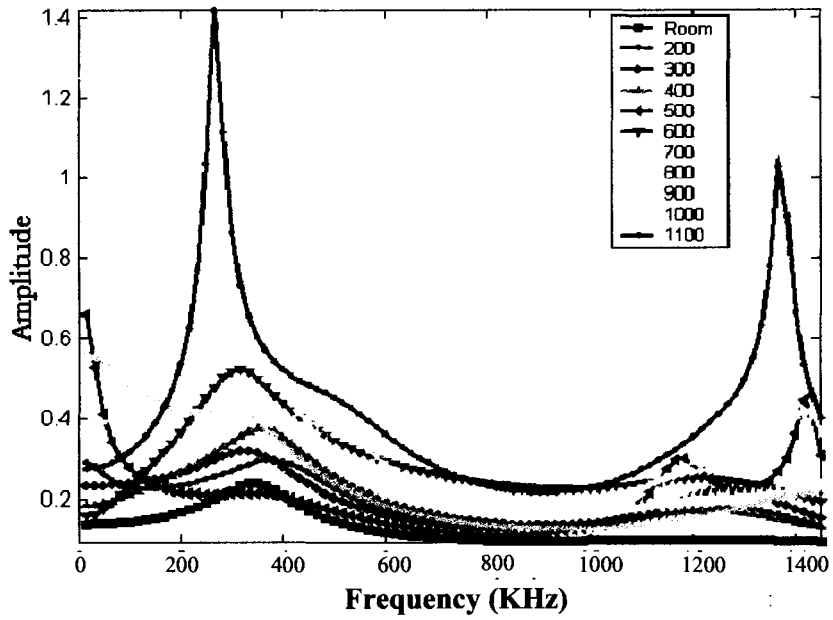


Figure 6.5 Amplitude versus frequency curve of polybenzimidazole sample from 200-1100°C

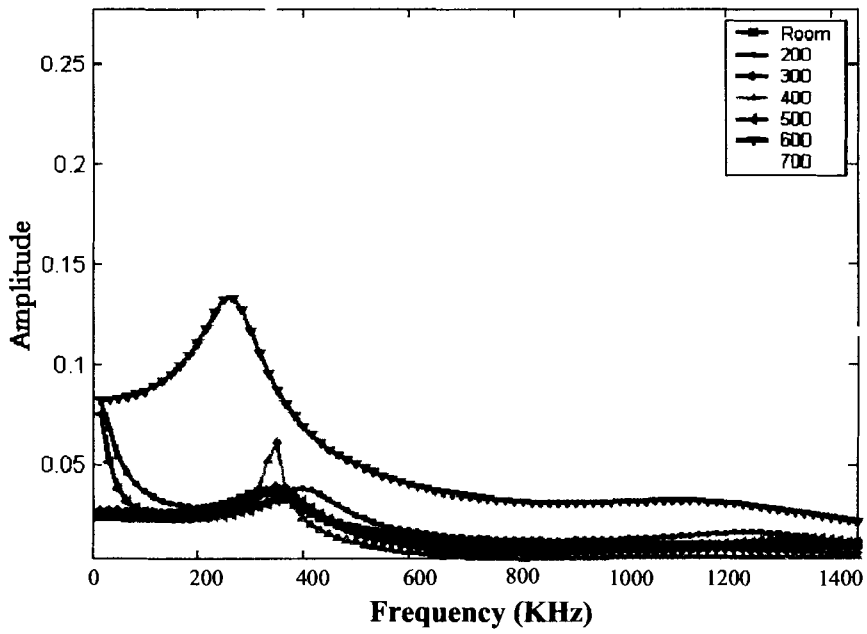


Figure 6.6 Amplitude versus frequency curve of borosilicate glass sample from 200-700°C

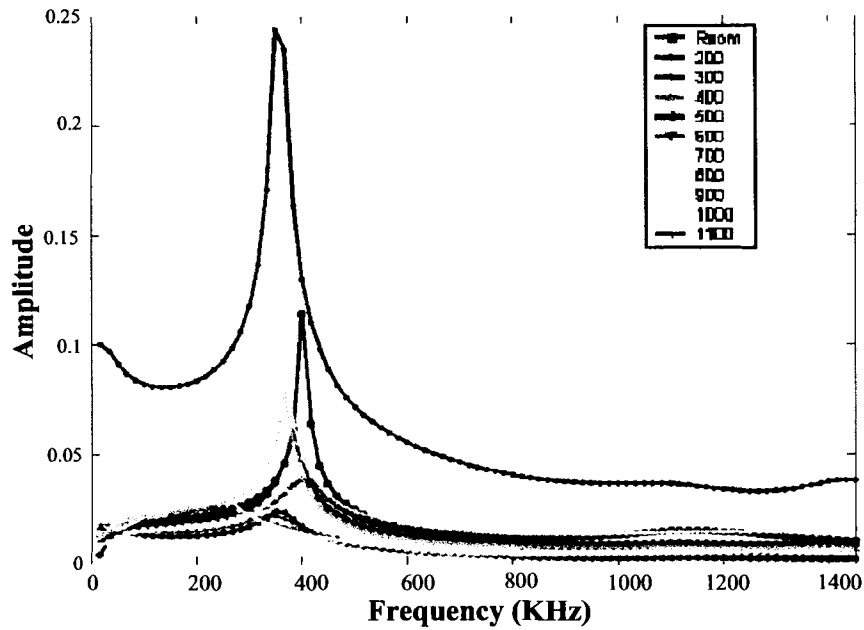


Figure 6.7 Amplitude versus frequency curve of silica glass sample from 200-1100°C

Plot obtained using a broad Hanning window includes peaks that are not necessary for coupling attenuation. The values of the variables used for broad Hanning window in the Hanning window equation (5.1) are $A = 1000$, $B = 400$, $C = 4300$, $D = 15000$. The Hanning window is narrowed to isolate only the first three peaks of the original signals. The values of the variables used for narrow Hanning window in the Hanning window equation (5.1) are $A = 800$, $B = 200$, $C = 3500$, $D = 15000$. The windowed signals are then deconvolved to give the new plots shown in figures 6.8 to 6.10. Only the plots for the samples that are selected in the screening are shown.

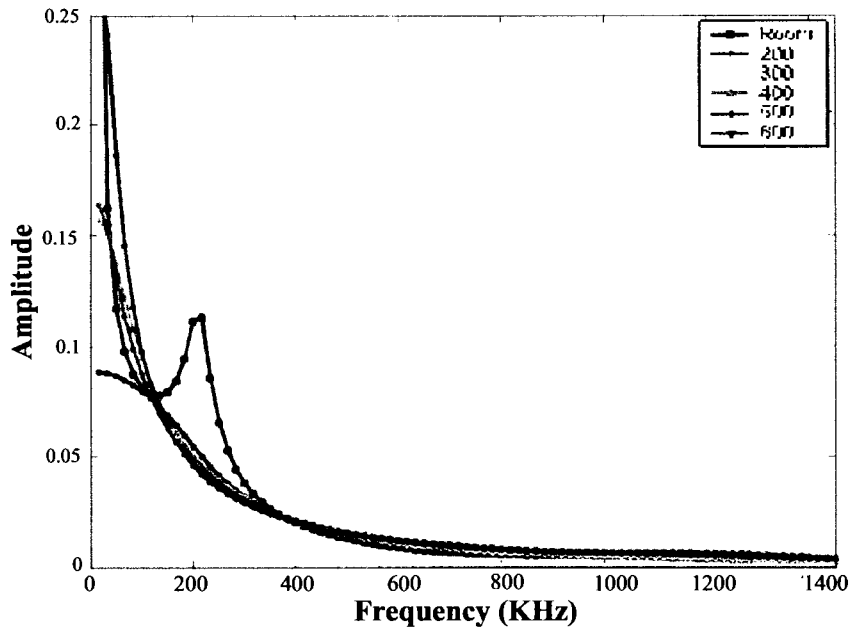


Figure 6.8 Amplitude versus frequency curve of aluminum from 200-600°C with narrow Hanning window

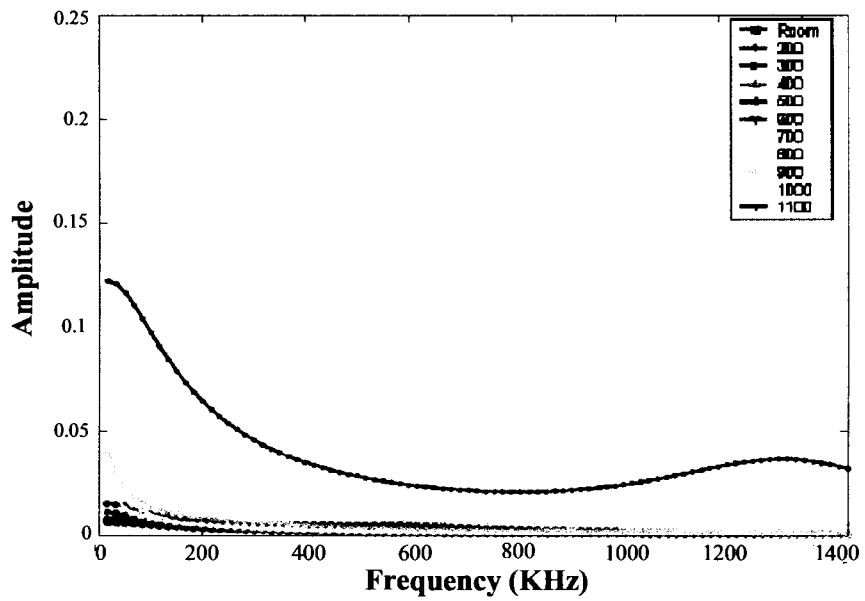


Figure 6.9 Amplitude versus frequency curve of silica glass from 200-1100°C with narrow Hanning window

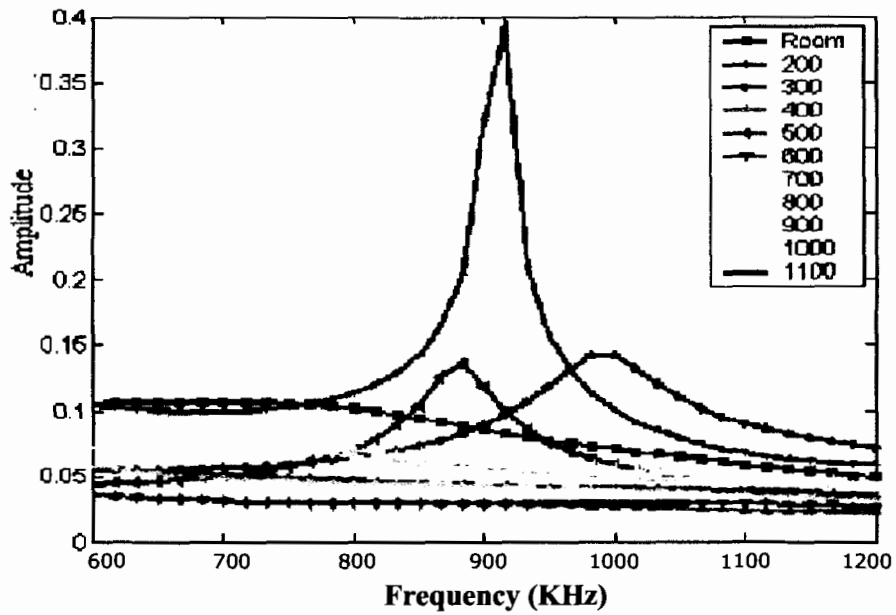


Figure 6.10 Amplitude versus frequency curve of gold from 200-1100°C with narrow Hanning window

6.3 Relative attenuation coefficient curves

The relative attenuation curves are plotted against the frequency. The relative attenuation found for the first aluminum foil, silica glass and gold foil are given in the figure 6.9, figure 6.10 and figure 6.11 respectively. The relative coefficient curves obtained for the remaining samples are given in the appendix.

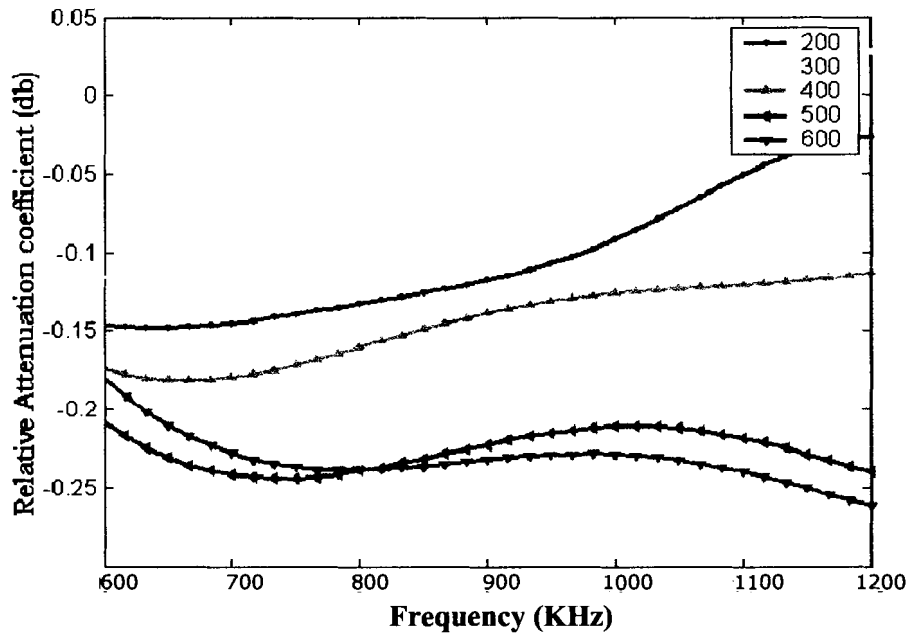


Figure 6.11 Relative attenuation coefficient curve for aluminum from 200-600°C

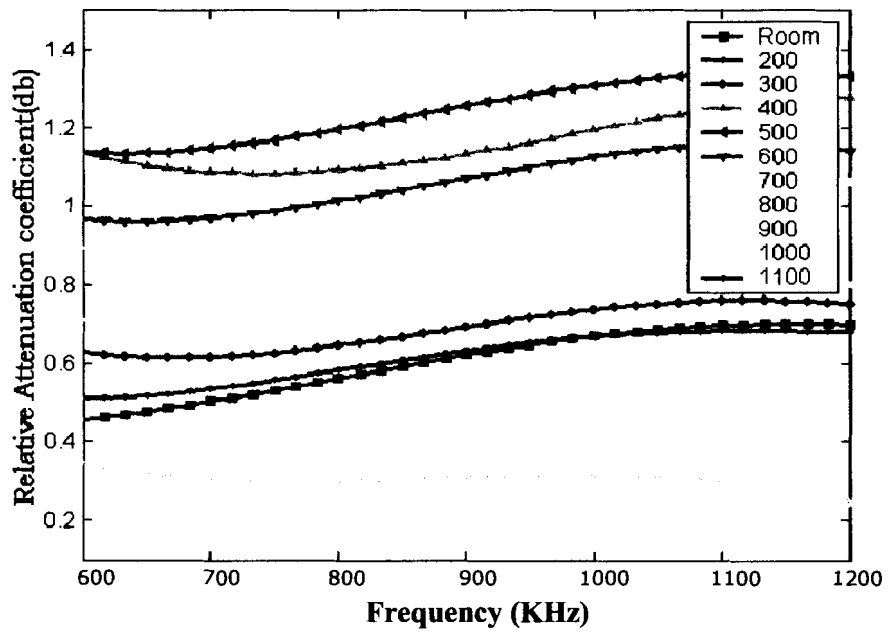


Figure 6.12 Relative attenuation coefficient curve for silica glass sample from 200-1100°C

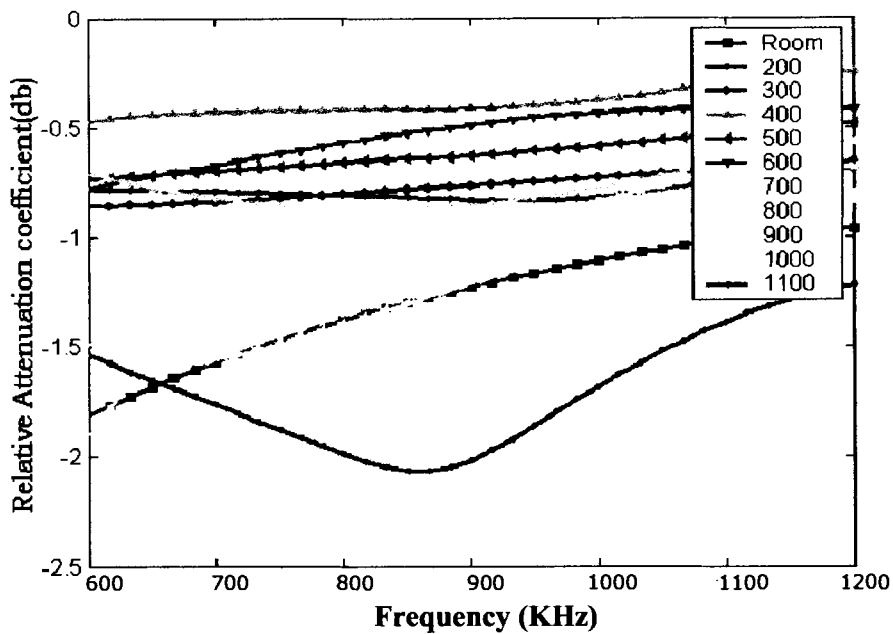


Figure 6.13 Relative attenuation coefficient curve for gold sample from 200-1100°C

6.4 Repeatability

From the initial experimental results on couplants the aluminum, gold and silica glass are selected for further consideration. These materials show lower attenuation change with an increase in temperature. The experiments with aluminum, gold and silica glass are repeated three times to test the repeatability with these couplants. The average of the relative attenuation coefficient value at each temperature of the three samples of selected couplants are given as error bars on the following figures.

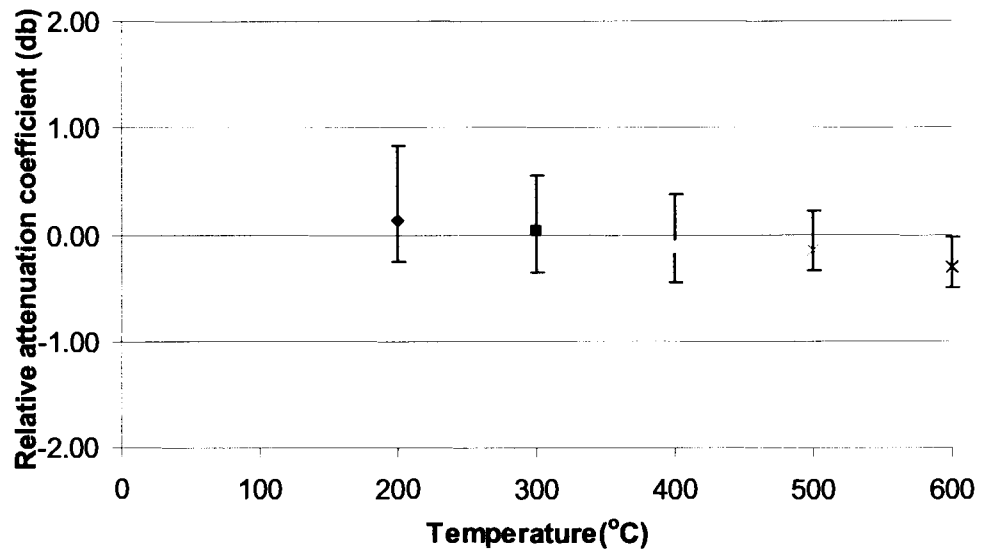


Figure 6.14 Error bar showing range of data for three aluminum samples tested from 200-600°C

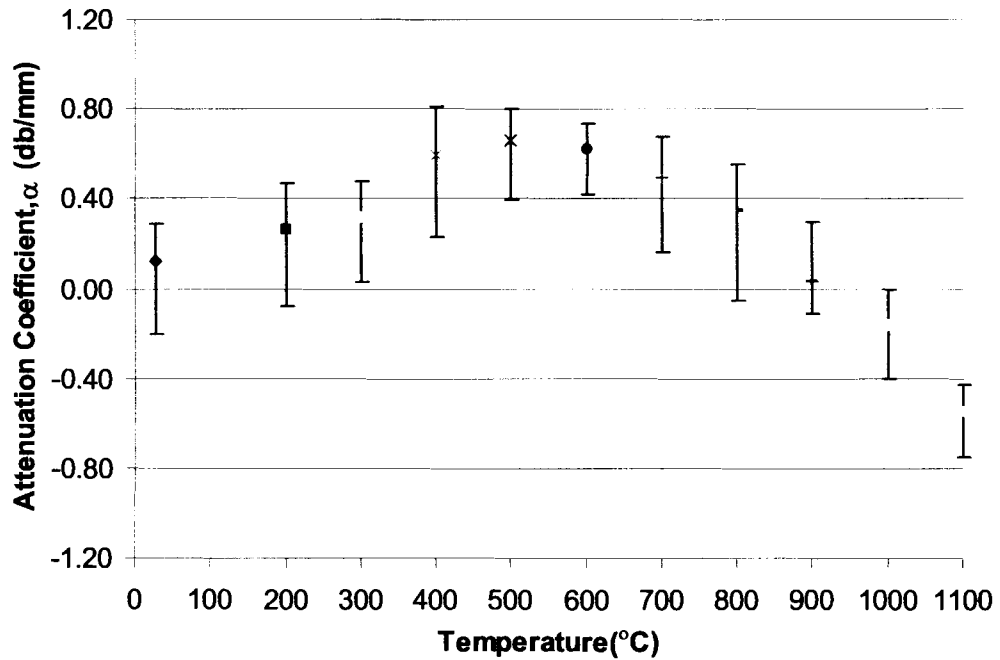


Figure 6.15 Error bar showing range of data for three silica glass samples tested from 200-1100°C

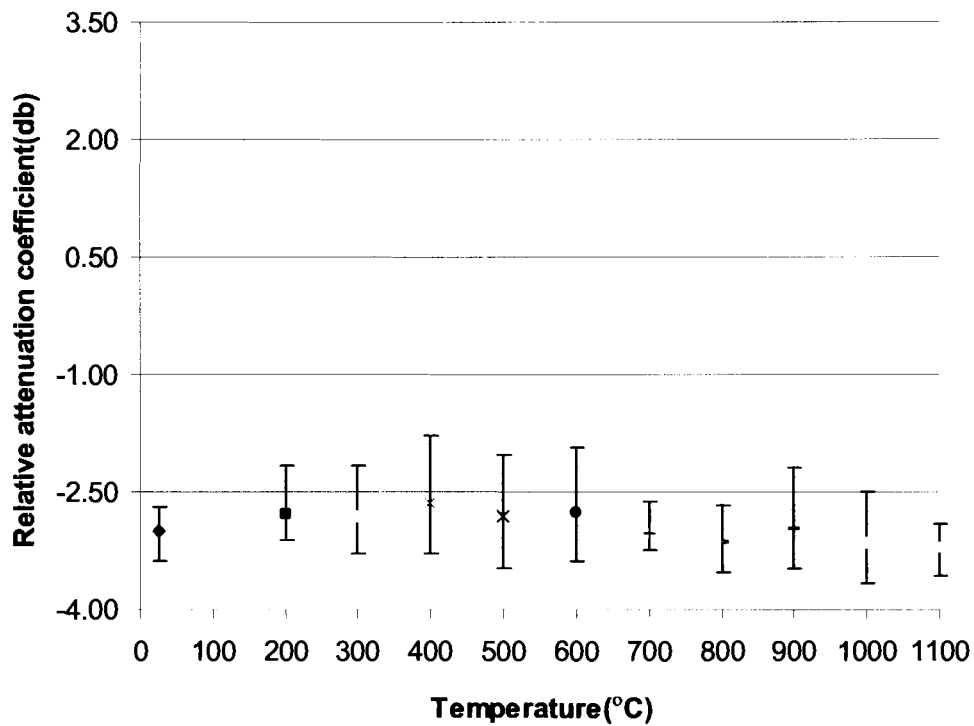


Figure 6.16 Error bar showing range of data for three gold samples tested from 200-1100°C

6.5 Average relative attenuation coefficient over a range of temperatures

The average of relative attenuation coefficients of each sample over a range of temperatures from temperatures 200 to 600°C and from temperatures 200 to 1100°C are shown in the following bar charts.

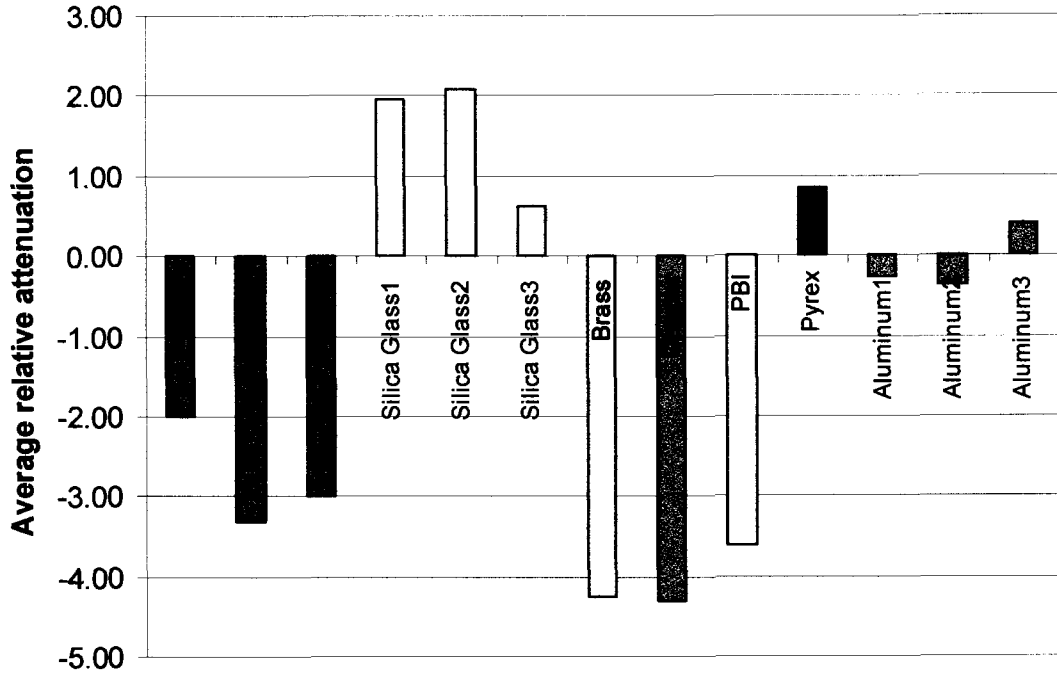


Figure 6.17 Average relative attenuation for different samples (0-600°C)

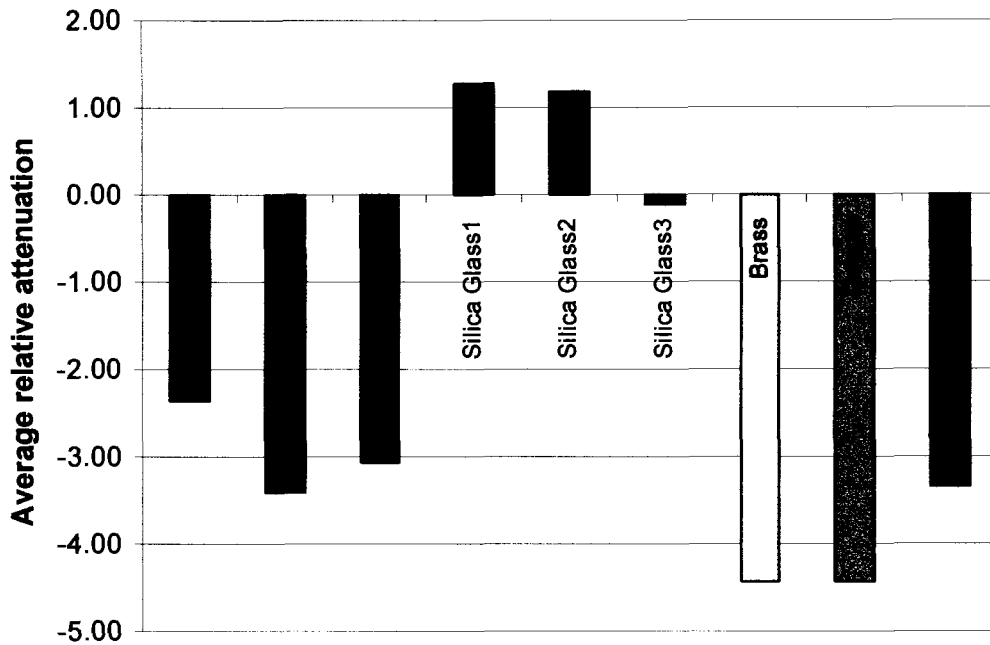


Figure 6.18 Average relative attenuation for different samples (0-1100°C)

6.6 Conclusions

From the relative attenuation graphs above, aluminum appears to be a good couplant over a range from 20 to 600°C, gold over a range from 20 to 1000°C and silica glass over a range of 20 to 1000°C. The expected variation in the signal amplitude due to coupling when using gold is approximately .4 dB greater than would be expected for aluminum over the temperature range of 20 to 600°C. Silica glass over the same range of 20 to 600°C has a variation in coupling which is approximately the same as gold. However silica introduces more complexity since it is only available in standard 1/8-inch thickness, which is much greater than the thickness of the metal foils. Thus attenuation measurements would have to be performed for a finite thickness-coupling layer, thereby increasing the complexity of the deconvolution algorithm. So the recommended couplant for use at temperatures from 20 to 600°C is aluminum foil.

For higher temperatures from 20 to 1100°C, gold would be the best choice. Though the use of PBI fabric resulted in the same signal attenuation as gold, at higher temperatures the PBI fabric contaminates the test sample. Copper and brass are less desirable because the signal attenuation is slightly higher. Because of the extremely high attenuation of the signal in the sample, it is critical that a couplant be used that maximize the amplitude of the received signal. In this case the difference between copper and brass and the gold is approximately 1.2 dB, or in other word the signal using the gold couplant is 1.15 times greater than

would be obtained with the brass or copper. The aluminum foil cannot be used at higher temperatures because the melting point of aluminum (approximately 625°C) is below the operating temperature of the furnace. Liquid aluminum is not a good couplant since it does not wet many of the surfaces that would be tested. With the previously described difficulties with the silica glass, the only remaining option for a higher temperature couplant is gold.

REFERENCES

- Blodgett, D. W., Baldwin, K. C., and Spicer, J. B., 1998. Measurement of High Temperature Elastic Moduli of Infrared Transparent Materials, PHYSICS AND ASTRONOMY: Mechanics, Conference Proceedings, Aug 1998.
- Bunker, S.P., 2002. Evaluation of Dynamic properties of Carbon-carbon Composite at Elevated Temperatures, Unpublished Master's thesis, University of Maine.
- Cracknell, A.P., 1980 *Ultrasonics*, London: Wykeham Publication Ltd.
- Dual, J., 2001. Dynamic Methods for Measuring the Elastic Properties of Solids, *Handbook of Elastic Properties of Solids, Liquids and Gases*, vol. I, 2001
- Fukuhara, M. and Sanpei, A., 1994. High Temperature-Elastic Moduli and Internal Dilational and Shear Frictions of Fused Quartz, *Japanese Journal of Applied Physics*, vol. 33, 1994
- Joon-Hyun Lee, Sang-Woo Choi, Nondestructive Characterisation of Carbon/Carbon Brake Disks Using Ultrasonics, <<http://www.ndt.net/article/apcndt01/papers/1109/1109.htm>>
- Karpur, P., Brian Frock and Bhagat, P.K., 1990. Wiener Filtering for Image Enhancement in Ultrasonic Nondestructive Evaluation, *Materials Evaluation*, 48(11): 1374-1379, Nov 1990.
- Krautkramer, J. and Krautkramer, H., 1975. *Ultrasonic testing of materials (Third, revised edition)*. New York: Springer-Verlag, Inc.

- Lynnworth, L.C., 1989. *Ultrasonic measurements for process control : theory, techniques, applications*. San Diego: Academic Press, Inc.
- Peterson, M.L., 1996. A Method for Increased Accuracy of the Measurement of Relative Phase Velocity, *Ultrasonics*, vol. 35, 1996
- Peterson, M.L., 1994. A Signal Processing Technique for Measurement of Multimode Waveguide Signals: An Application to Monitoring Reaction Bonding in Silicon Nitride, *Nondestructive Evaluation*, 1994, New York: Springer-Verlag, Inc.
- Peterson, M.L., 1999. Prediction of Longitudinal Disturbances in a Multimode Cylindrical Waveguide, *Experimental Mechanics*, v 39, Mar, 1999.
- Redwood, M. R., 1960. *Mechanical Waveguides*, New York: Pergamon Press.
- Schmerr, Jr., L. W., 1998. *Fundamental of Ultrasonic Nondestructive Evaluation; A Modeling Approach*. New York: Plenum Press.
- Thurston, R. N., 1978. Elastic Waves in Rods and Clad Rods, *Journal of the Acoustical Society of America*, v 64, 1978.

APPENDIX A- Thermocouple temperatures (°C)

Furnace setting (°C)	Recorded thermocouple temperatures (°C)	
	<i>Thermocouple 1</i>	<i>Thermocouple 2</i>
100	30	83
200	30	96
300	30	269
400	30	355
500	30	445
600	30	531
700	30	610
800	30	710
900	30	795
1000	30	880
1100	30	960
Position (in)	0 (Transducer)	9

Table A.1 Thermocouple temperature recordings with sapphire rod

Furnace Setting	Recorded Thermocouple Temperatures (°C)						
800°C	30.4	209.5	665.92	795	810.21	810.2	808.47
900°C	37.4	243	754	890.7	905.9	905.25	903.69
1000°C	38.9	281.2	846.6	987.7	1003.4	1002.2	1001
1100°C	46	324.5	939.2	1085	1102.6	1101.6	1100.7
Position (in)	trans.	0	4	8	12	16	20

Table A.2 Thermocouple temperature recordings with Fused Quartz rod

APPENDIX B – Ultrasonic system settings

The pulser settings:

The pulser Energy was set to 4 which is equal to 400volts

Damping was set to 3 which is equal to 50ohms

Built in pre-amp was set to 50db

The pre-amp settings:

Pre-amp used is set to 60db gain.

The oscilloscope settings:

Trigger position is set to 0%.

Number of points per record are 15000.

Sampling rate is 250 Mega samples per second.

Time delay is 195 microseconds.

Signal averaging is set to 50 signals.

APPENDIX C- Solution for the simultaneous equations

$$P_i + P_r = P_t \quad \text{C.1}$$

$$\left(\frac{ik_1}{\rho_1}\right)P_i - \left(\frac{ik_1}{\rho_1}\right)P_r = \left(\frac{ik_2}{\rho_2}\right)P_t \quad \text{C.2}$$

Dividing equation C.2 with ik_1 and multiplying with ρ_1 the equation becomes

$$P_i - P_r = \left(\frac{k_2}{\rho_2}\right)\left(\frac{\rho_1}{k_1}\right)P_t \quad \text{C.3}$$

Adding equations C.1 and C.3 we get,

$$P_i = \frac{2k_1\rho_2}{k_1\rho_2 + k_2\rho_1}P_t \quad \text{C.4}$$

Substituting the P_t in equation C.1 we obtain P_r of the form

$$P_r = \frac{k_1\rho_2 - k_2\rho_1}{k_1\rho_2 + k_2\rho_1}P_t \quad \text{C.5}$$

For plane harmonic wave motion at $x=0$, angular frequency ω is given as k_1c_1 in first medium and k_2c_2 in the second medium.

Therefore,

$$k_1c_1 = k_2c_2 \quad \text{C.6}$$

Substituting the k_1 from the equation C.6 into equations C.4 and C.5 we obtain

$$\frac{P_t}{P_i} = T_p = \frac{2\rho_2c_2}{\rho_1c_1 + \rho_2c_2} \quad \text{C.7}$$

$$\frac{P_r}{P_i} = R_p = \frac{\rho_2c_2 - \rho_1c_1}{\rho_2c_2 + \rho_1c_1} \quad \text{C.8}$$

APPENDIX D- Signal processing Matlab programs

Preparation of Signal for Deconvolution (Through transmission)

```
clear W2
ref=textread('C:\usr\Amala\Couplant\coup Silica Glass\coup
  SIGlass2\1100\1100A.dat');

ref(:,2) = ref(:,2)-ref(10,2); %Lines up vertical to zero
ref(:,2) = ref(:,2)./(1000); %Divides by 1000 because of Amp set on 60db

A = 1000; %Number of zeroes at beginning of signal
B = 400; %1/2 of the Hanning Window used judged by looking at plot of
  signal
C = 4300; %Data point to end window
D = 15000; %Total number of Data points recorded

W1 = Hanning(2*B);
W2(1:A)=0;
W2((A+1):(A+B))=W1(1:B);
W2((A+1+B):(C-B))=1;
W2((C-B+1):C) = W1((B+1):(2*B));
W2((C+1):D) = 0;

newref(:,2)=ref(:,2).*W2'; %Windows Amplitude column in ref
newref(:,1)=ref(:,1); %Copies over time column

y=[newref(:,1)';newref(:,2)'];

fid=fopen('C:\usr\Amala\Couplant\coup Silica glass\coup
  SIGlass2\XprepOUT\1100\1100A.dat','w');
fprintf(fid,'%8.4e %8.4e\n',y);
status=fclose(fid);

subplot(2,1,1);
plotyy(ref(:,1),ref(:,2),ref(:,1),W2);
title('Original Signal with Hanning Window');
xlabel('Time(s)')

subplot(2,1,2);
plot(newref(:,2));
title('Windowed Signal');
xlabel('Time(s)');
ylabel('Voltage(v)');
```

Preparation of Signal for Deconvolution (Pulse-echo transmission)

```
clear W2
ref=textread('C:\usr\Amala\Couplant\coup Silica Glass\coup
SIGlass2\1100\1100B.dat');

ref(:,2) = ref(:,2)-ref(10,2);    %Lines up vertical to zero
ref(:,2) = ref(:,2)./(10^2.5);    %Divides by 10^2.5 because of Pulser Amp set on
50db

A = 900;        %Number of zeroes at beginning of signal
B = 400;        %1/2 of the Hanning Window used judged by looking at plot of
signal
C = 4100;       %Data point to end window
D = 15000;      %Total number of Data points recorded

W1 = Hanning(2*B);
W2(1:A)=0;
W2((A+1):(A+B))=W1(1:B);
W2((A+1+B):(C-B))=1;
W2((C-B+1):C) = W1((B+1):(2*B));
W2((C+1):D) = 0;

newref(:,2)=ref(:,2).*W2';    %Windows Amplitude column in ref
newref(:,1)=ref(:,1);        %Copies over time column

y=[newref(:,1);newref(:,2)'];

fid=fopen('C:\usr\Amala\Couplant\coup Silica Glass\coup
SIGlass2\XprepOUT\1100\1100B.dat','w');
fprintf(fid,'%8.4e %8.4e\n',y);
status=fclose(fid);

subplot(2,1,1);
plotyy(ref(:,1),ref(:,2),ref(:,1),W2);
title('Original Signal');
xlabel('Time(s)');

subplot(2,1,2);
plot(newref(:,2));
title('Windowed Signal');
xlabel('Time(s)');
ylabel('Voltage(v)');
```

Program to graph new signals

```
clear;
```

```
REFRoom = textread('C:\usr\Amala\Couplant\coup Silica Glass\coup  
SIGlass1\XprepOUT\RoomW\ARoomA.dat');  
REF2=textread('C:\usr\Amala\Couplant\coup Silica Glass\coup  
SIGlass1\XprepOUT\200\A200A.dat');  
REF3=textread('C:\usr\Amala\Couplant\coup Silica Glass\coup  
SIGlass1\XprepOUT\300\A300A.dat');  
REF4=textread('C:\usr\Amala\Couplant\coup Silica Glass\coup  
SIGlass1\XprepOUT\400\A400A.dat');  
REF5=textread('C:\usr\Amala\Couplant\coup Silica Glass\coup  
SIGlass1\XprepOUT\500\A500A.dat');  
REF6=textread('C:\usr\Amala\Couplant\coup Silica Glass\coup  
SIGlass1\XprepOUT\600\A600A.dat');  
REF7=textread('C:\usr\Amala\Couplant\coup Silica Glass\coup  
SIGlass1\XprepOUT\700\A700A.dat');  
REF8=textread('C:\usr\Amala\Couplant\coup Silica Glass\coup  
SIGlass1\XprepOUT\800\A800A.dat');  
REF9=textread('C:\usr\Amala\Couplant\coup Silica Glass\coup  
SIGlass1\XprepOUT\900\A900A.dat');  
REF10=textread('C:\usr\Amala\Couplant\coup Silica Glass\coup  
SIGlass1\XprepOUT\1000\A1000A.dat');  
REF11=textread('C:\usr\Amala\Couplant\coup Silica Glass\coup  
SIGlass1\XprepOUT\1100\A1100A.dat');
```

```
subplot(11,1,1);  
plot(REFRoom(:,2));  
% axis([0 15000 -.000005 .000005]);  
ylabel('Room');
```

```
subplot(11,1,2);  
plot(REF2(:,2));  
% axis([0 15000 -.000005 .000005]);  
ylabel('200');
```

```
subplot(11,1,3);  
plot(REF3(:,2));  
% axis([0 15000 -.000005 .000005]);  
ylabel('300');  
subplot(11,1,4);
```

```
plot(REF4(:,2));
% axis([0 15000 -.000005 .000005]);
ylabel('400');

subplot(11,1,5);
plot(REF5(:,2));
% axis([0 15000 -.000005 .000005]);
ylabel('500');

subplot(11,1,6);
plot(REF6(:,2));
% axis([0 15000 -.000005 .000005]);
ylabel('600');

subplot(11,1,7);
plot(REF7(:,2));
% axis([0 15000 -.000005 .000005]);
ylabel('700');

subplot(11,1,8);
plot(REF8(:,2));
% axis([0 15000 -.000005 .000005]);
ylabel('800');
xlabel('Time');

subplot(11,1,9);
plot(REF9(:,2));
% axis([0 15000 -.000005 .000005]);
ylabel('900');

subplot(11,1,10);
plot(REF10(:,2));
% axis([0 15000 -.000005 .000005]);
ylabel('1000');

subplot(11,1,11);
plot(REF11(:,2));
% axis([0 15000 -.000005 .000005]);
ylabel('1100');
```

Deconvolution program

```
clear all;
X=textread('C:\usr\Amala\Couplant\coup Silica Glass\coup
SIGlass3\XprepOUT\1100\1100A.dat');
X1=textread('C:\usr\Amala\Couplant\coup Silica Glass\coup
SIGlass3\XprepOUT\1100\1100C.dat');
Y=textread('C:\usr\Amala\Couplant\coup Silica Glass\coup
SIGlass3\XprepOUT\1100\1100B.dat');
Y1=textread('C:\usr\Amala\Couplant\coup Silica Glass\coup
SIGlass3\XprepOUT\1100\1100D.dat');
ampfile = fopen('C:\usr\Amala\Couplant\coup Silica Glass\coup
SIGlass3\XprepOUT\1100\1100_A.dat','w');

Xt = X(:,2);
Xw = fft(Xt,2^16);

X1t = X1(:,2);
X1w = fft(X1t,2^16);

Yt = Y(:,2);
Yw = fft(Yt,2^16);

Y1t = Y1(:,2);
Y1w = fft(Y1t,2^16);

R= -0.073123078

F = sqrt(R*R);
Hw = F*(sqrt((Xw.*X1w)./(Yw.*Y1w)));
Hwr = real(Hw);
Hwim = imag(Hw);

dt=X(2)-X(1);

m=max(size(X));

for n=1:m
    f(n)=1*n/(m*dt);
    if f(n)<=2000000;
        fprintf(ampfile,' %f %f %f
%f\r\n',f(n),Hwr(n,1),Hwim(n,1),sqrt((Hwr(n,1)*Hwr(n,1)+(Hwim(n,1)*Hwim(n,1))));
    end
end
```

```

end
a=textread('C:\usr\Amala\Couplant\coup Silica Glass\coup
SIGlass3\XprepOUT\1100\1100_A.dat');
plot(a(:,1),a(:,4));
% axis([600000 1200000 0 0.25]);
xlabel('Frequency in Hz')
ylabel('Amplitude')
title('Attenuation Curve')

```

Program to plot graphs after deconvolution of signals

```

RW=textread('C:\usr\Amala\Couplant\coup
Gold\Gold1\XprepOUT\Room\RoomN.dat');
T2=textread('C:\usr\Amala\Couplant\coup
Gold\Gold1\XprepOUT\200\200N.dat');
T3=textread('C:\usr\Amala\Couplant\coup
Gold\Gold1\XprepOUT\300\300N.dat');
T4=textread('C:\usr\Amala\Couplant\coup
Gold\Gold1\XprepOUT\400\400N.dat');
T5=textread('C:\usr\Amala\Couplant\coup
Gold\Gold1\XprepOUT\500\500N.dat');
T6=textread('C:\usr\Amala\Couplant\coup
Gold\Gold1\XprepOUT\600\600N.dat');
T7=textread('C:\usr\Amala\Couplant\coup
Gold\Gold1\XprepOUT\700\700N.dat');
T8=textread('C:\usr\Amala\Couplant\coup
Gold\Gold1\XprepOUT\800\800N.dat');
T9=textread('C:\usr\Amala\Couplant\coup
Gold\Gold1\XprepOUT\900\900N.dat');
T10=textread('C:\usr\Amala\Couplant\coup
Gold\Gold1\XprepOUT\1000\1000N.dat');
T11=textread('C:\usr\Amala\Couplant\coup
Gold\Gold1\XprepOUT\1100\1100N.dat');

plot(RW(:,1),RW(:,4),'-ms','LineWidth',2,...
      'MarkerEdgeColor','m',...
      'MarkerSize',3);

hold on
plot(T2(:,1),T2(:,4),'-b*','LineWidth',2,...
      'MarkerEdgeColor','b',...
      'MarkerSize',3);

hold on
plot(T3(:,1),T3(:,4),'-d','color',[0.2500 0.2500 0.2500],'LineWidth',2,...

```

```

        'MarkerEdgeColor',[0.2500 0.2500 0.2500],...
        'MarkerSize',3);

hold on
plot(T4(:,1),T4(:,4),'-c^','LineWidth',2,...
     'MarkerEdgeColor','c',...
     'MarkerSize',3);

hold on
plot(T5(:,1),T5(:,4),'-<','color',[0,0.554,0],'LineWidth',2,...
     'MarkerEdgeColor',[0,0.554,0],...
     'MarkerSize',3);

hold on
plot(T6(:,1),T6(:,4),'-gV','LineWidth',2,...
     'MarkerEdgeColor','g',...
     'MarkerSize',3);

hold on
plot(T7(:,1),T7(:,4),'->','color',[0.761,0.851,0.671],'LineWidth',2,...
     'MarkerEdgeColor',[0.761,0.851,0.671],...
     'MarkerSize',3);

hold on
plot(T8(:,1),T8(:,4),'-yp','LineWidth',2,...
     'MarkerEdgeColor','y',...
     'MarkerSize',4);

hold on;
plot(T9(:,1),T9(:,4),'-o','color',[1.0,0.706,0],'LineWidth',2,...
     'MarkerEdgeColor',[1.0,0.706,0],...
     'MARKERSIZE',3);

hold on;
plot(T10(:,1),T10(:,4),'-h','color',[1.000,0.655,0.608],'LineWidth',2,...
     'MarkerEdgeColor',[1.000,0.655,0.608],...
     'MarkerSize',3);

hold on;
plot(T11(:,1),T11(:,4),'-r+','LineWidth',2,...
     'MarkerEdgeColor','r',...
     'MarkerSize',3);
axis([0 1450000 0 0.4]);
Legend('Room','200','300','400','500','600','700','800','900','1000','1100');
xlabel('Frequency(Hz)','FontName','Bookman old
style','FontSize',0.5,'FontSize',12)
ylabel('Amplitude','FontName','Bookman old style','FontSize',0.5,'FontSize',12)

```

Relative attenuation curve

```
REF=textread('C:\USR\Amala\Couplant\coup Aluminum\coup
AL1\XprepOUT\RoomW\RoomN1.dat');
CR=textread('C:\USR\Amala\Couplant\coup
PBI\XprepOUT\Roomw\RoomN.dat');
C200=textread('C:\usr\Amala\Couplant\coup PBI\XprepOUT\200\200N.dat');
C300=textread('C:\USR\Amala\Couplant\coup PBI\XprepOUT\300\300N.dat');
C400=textread('C:\USR\Amala\Couplant\coup PBI\XprepOUT\400\400N.dat');
C500=textread('C:\USR\Amala\Couplant\coup PBI\XprepOUT\500\500N.dat');
C600=textread('C:\USR\Amala\Couplant\coup PBI\XprepOUT\600\600N.dat');
C700=textread('C:\USR\Amala\Couplant\coup PBI\XprepOUT\700\700N.dat');
C800=textread('C:\USR\Amala\Couplant\coup PBI\XprepOUT\800\800N.dat');
C900=textread('C:\USR\Amala\Couplant\coup PBI\XprepOUT\900\900N.dat');
C1000=textread('C:\USR\Amala\Couplant\coup
PBI\XprepOUT\1000\1000N.dat');
C1100=textread('C:\USR\Amala\Couplant\coup
PBI\XprepOUT\1100\1100N.dat');
%%%%%%%%%%Alpha
calculation%%%%%%%%%%
%%%
```

```
REFw=REF(:,4);
CRw=CR(:,4);
c1 = (CRw./REFw);
alpha1 = -log(c1);
```

```
C200w=C200(:,4);
c2 = (C200w./REFw);
alpha2 = -log(c2);
```

```
C300w=C300(:,4);
c3 = (C300w./REFw);
alpha3 = -log(c3);
```

```
C400w=C400(:,4);
c4 = (C400w./REFw);
alpha4 = -log(c4);
```

```
C500w=C500(:,4);
c5 = (C500w./REFw);
alpha5 = -log(c5);
```

```
C600w=C600(:,4);
c6 = (C600w./REFw);
alpha6 = -log(c6);
```

```
C700w=C700(:,4);
c7 = (C700w./REFw);
alpha7 = -log(c7);
```

```
C800w=C800(:,4);
c8 = (C800w./REFw);
alpha8 = -log(c8);
```

```
C900w=C900(:,4);
c9 = (C900w./REFw);
alpha9 = -log(c9);
```

```
C1000w=C1000(:,4);
c10 = (C1000w./REFw);
alpha10 = -log(c10);
```

```
C1100w=C1100(:,4);
c11 = (C1100w./REFw);
alpha11 = -log(c11);
```

plots

```
A1=[REF(:,1);alpha1'];
A2=[REF(:,1);alpha2'];
A3=[REF(:,1);alpha3'];
A4=[REF(:,1);alpha4'];
A5=[REF(:,1);alpha5'];
A6=[REF(:,1);alpha6'];
A7=[REF(:,1);alpha7'];
A8=[REF(:,1);alpha8'];
A9=[REF(:,1);alpha9'];
A10=[REF(:,1);alpha10'];
A11=[REF(:,1);alpha11'];
```

```
plot(REF(:,1),alpha1,'-ms','LineWidth',2,...
      'MarkerEdgeColor','m',...
      'MarkerSize',3);
```

```
hold on;
plot(A2(1,:),A2(2,:),'-b*','LineWidth',2,...
      'MarkerEdgeColor','b',...
      'MarkerSize',3);
```

```
hold on;
```

```
plot(A3(1,:),A3(2,:),'-d','color',[0.2500 0.2500 0.2500],'LineWidth',2,...  
     'MarkerEdgeColor',[0.2500 0.2500 0.2500],...  
     'MarkerSize',3);
```

```
hold on;  
plot(A4(1,:),A4(2,:),'-c^','LineWidth',2,...  
     'MarkerEdgeColor','c',...  
     'MarkerSize',3);
```

```
hold on;  
plot(A5(1,:),A5(2,:),'-<','color',[0,0.554,0],'LineWidth',2,...  
     'MarkerEdgeColor',[0,0.554,0],...  
     'MarkerSize',3);
```

```
hold on;  
plot(A6(1,:),A6(2,:),'-gV','LineWidth',2,...  
     'MarkerEdgeColor','g',...  
     'MarkerSize',3);
```

```
hold on;  
plot(A7(1,:),A7(2,:),'->','color',[0.761 0.851 0.671],'LineWidth',2,...  
     'MarkerEdgeColor',[0.761 0.851 0.671],...  
     'MarkerSize',3);
```

```
hold on;  
plot(A8(1,:),A8(2,:),'-yp','LineWidth',2,...  
     'MarkerEdgeColor','y',...  
     'MarkerSize',3);
```

```
hold on;  
plot(A9(1,:),A9(2,:),'-o','color',[1.0,0.706,0],'LineWidth',2,...  
     'MarkerEdgeColor',[1.0,0.706,0],...  
     'MarkerSize',3);
```

```
hold on;  
plot(A10(1,:),A10(2,:),'-h','color',[1.000,0.655,0.608],'LineWidth',2,...  
     'MarkerEdgeColor',[1.000,0.655,0.608],...  
     'MarkerSize',3);
```

```

hold on;
plot(A11(1,:),A11(2,:),'-r+','LineWidth',2,...
      'MarkerEdgeColor','r',...
      'MarkerSize',3);

Legend('Room','200','300','400','500','600','700','800','900','1000','1100');
xlabel('Frequency(Hz)','FontName','Bookman old
style','FontSize',0.5,'FontSize',12)
ylabel('Relative Attenuation coefficient(db)','FontName','Bookman old
style','FontSize',0.5,'FontSize',12)
axis([600000 1200000 -Inf Inf]);
title('Relative attenuation curve for PBI')

```

DataOutput

```

fid=fopen('C:\usr\Amala\Thesis\PBI\RAC1.dat','w');
fprintf(fid,'%8.4e %8.4e\n',A1);
status=fclose(fid);

```

```

fid=fopen('C:\usr\Amala\Thesis\PBI\RAC2.dat','w');
fprintf(fid,'%8.4e %8.4e\n',A2);
status=fclose(fid);

```

```

fid=fopen('C:\usr\Amala\Thesis\PBI\RAC3.dat','w');
fprintf(fid,'%8.4e %8.4e\n',A3);
status=fclose(fid);

```

```

fid=fopen('C:\usr\Amala\Thesis\PBI\RAC4.dat','w');
fprintf(fid,'%8.4e %8.4e\n',A4);
status=fclose(fid);

```

```

fid=fopen('C:\usr\Amala\Thesis\PBI\RAC5.dat','w');
fprintf(fid,'%8.4e %8.4e\n',A5);
status=fclose(fid);

```

```

fid=fopen('C:\usr\Amala\Thesis\PBI\RAC6.dat','w');
fprintf(fid,'%8.4e %8.4e\n',A6);
status=fclose(fid);

```

```

fid=fopen('C:\usr\Amala\Thesis\PBI\RAC7.dat','w');
fprintf(fid,'%8.4e %8.4e\n',A7);
status=fclose(fid);

```

```

fid=fopen('C:\usr\Amala\Thesis\PBI\RAC8.dat','w');
fprintf(fid,'%8.4e %8.4e\n',A8);

```

```
status=fclose(fid);
```

```
fid=fopen('C:\usr\Amala\Thesis\PBI\RAC9.dat','w');  
fprintf(fid,'%8.4e %8.4e\n',A9);  
status=fclose(fid);
```

```
fid=fopen('C:\usr\Amala\Thesis\PBI\RAC10.dat','w');  
fprintf(fid,'%8.4e %8.4e\n',A10);  
status=fclose(fid);
```

```
fid=fopen('C:\usr\Amala\Thesis\PBI\RAC11.dat','w');  
fprintf(fid,'%8.4e %8.4e\n',A11);  
status=fclose(fid);
```

APPENDIX E- Samples of through and pulse-echo signals

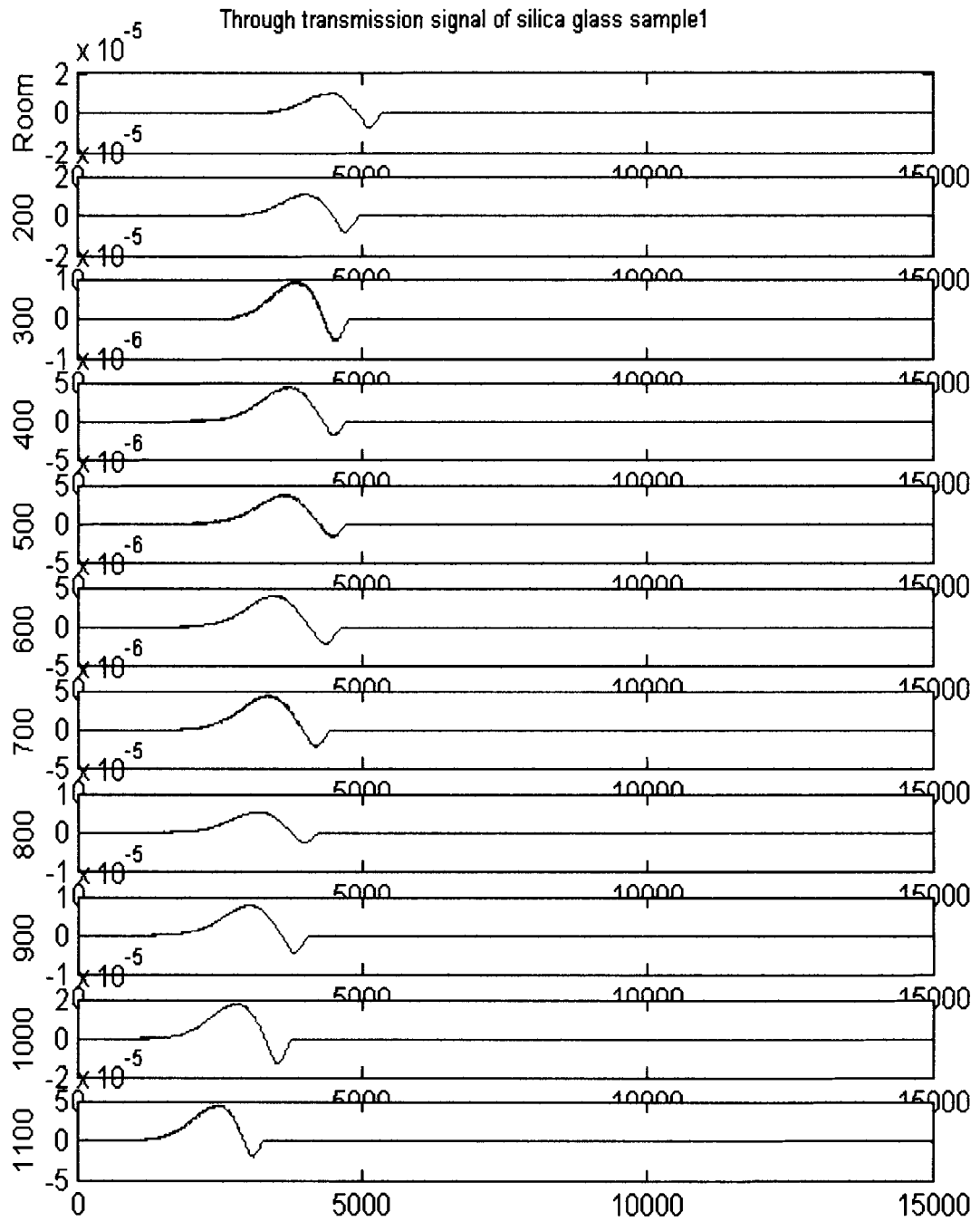


Figure E.1. Through transmission signal for silica glass sample 1.

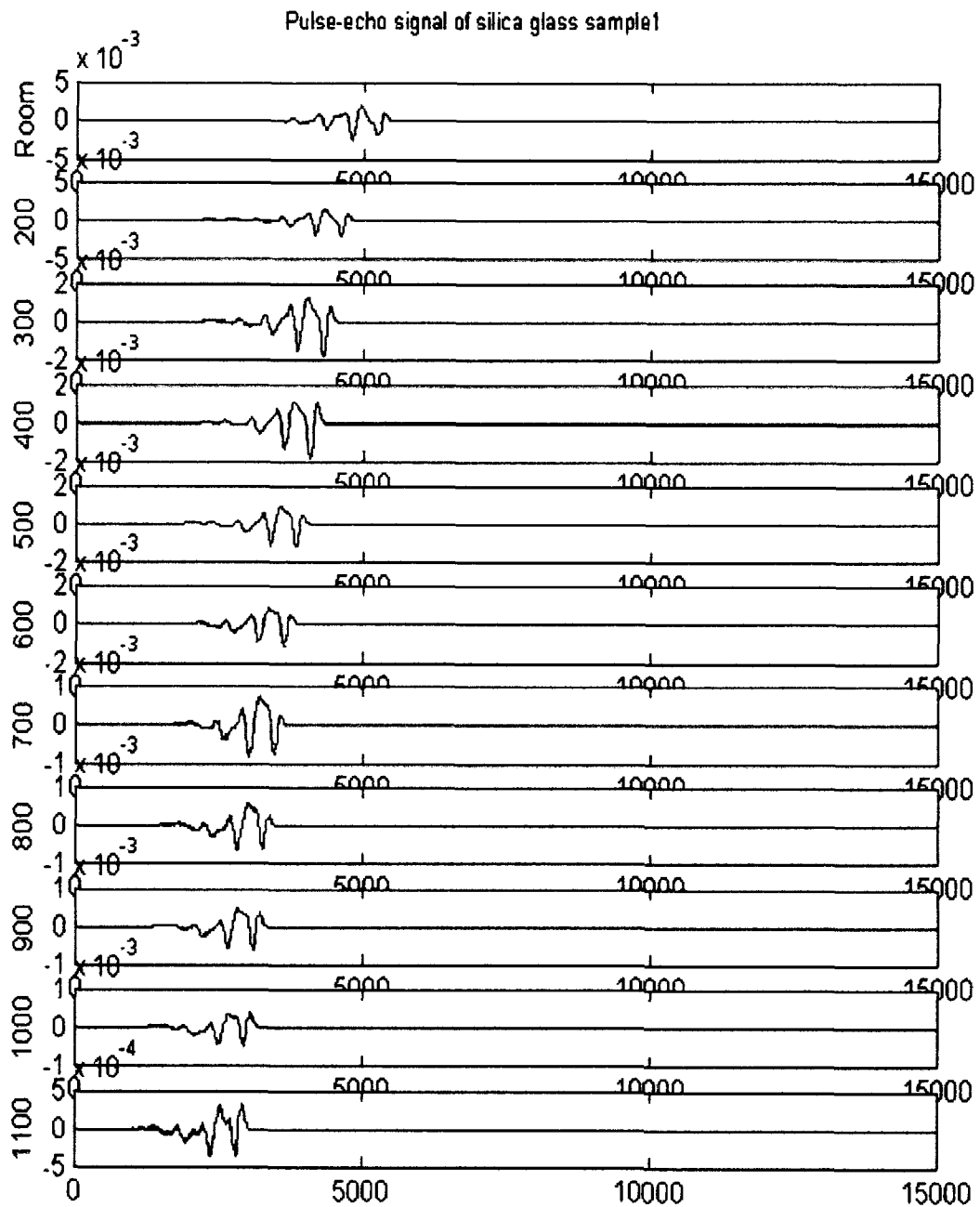


Figure E.2 Pulse echo signal for silica glass sample 1.

**APPENDIX F – Derivation of the response of the couplant material by
deconvolution method**

$$\frac{X(\omega)X'(\omega)}{Y(\omega)Y'(\omega)} = \frac{\left(A_{it}(\omega)H_{ib}(\omega)H_b(\omega)H_c(\omega)H_b(\omega)H_{bt}'(\omega)H_{bt}'(\omega)A_{2r}(\omega) \right) \left(A_{2t}(\omega)H_{ib}'(\omega)H_b'(\omega)H_c(\omega)H_b(\omega)H_{bt}'(\omega)H_{bt}'(\omega)A_{1r}(\omega) \right)}{\left(A_{it}(\omega)H_{ib}(\omega)H_b(\omega)R_{bc}(\omega)H_b(\omega)H_{bt}'(\omega)A_{1r}(\omega) \right) \left(A_{2t}(\omega)H_{ib}'(\omega)H_b'(\omega)R_{bc}'(\omega)H_b'(\omega)H_{bt}'(\omega)H_{bt}'(\omega)A_{2r}(\omega) \right)}$$

$$= \frac{\left(A_{it}(\omega)H_{ib}(\omega)H_b(\omega)H_c(\omega)H_b(\omega)H_{bt}'(\omega)H_{bt}'(\omega)A_{2r}(\omega) \right) \left(A_{2t}(\omega)H_{ib}'(\omega)H_b'(\omega)H_c(\omega)H_b(\omega)H_{bt}'(\omega)H_{bt}'(\omega)A_{1r}(\omega) \right)}{\left(A_{1r}'(\omega)H_{ib}'(\omega)H_b'(\omega)R_{bc}(\omega)H_b(\omega)H_{bt}'(\omega)A_{1r}(\omega) \right) \left(A_{2t}(\omega)H_{ib}'(\omega)H_b'(\omega)R_{bc}'(\omega)H_b'(\omega)H_{bt}'(\omega)H_{bt}'(\omega)A_{2r}(\omega) \right)}$$

Assuming $R_{bc} = R'_{bc}$,

Response of the couplant material:

$$H_c(\omega) = \sqrt{(R_{bc})^2 \left(\frac{X(\omega)X'(\omega)}{Y(\omega)Y'(\omega)} \right)}$$

APPENDIX G- Sample data sheet for reflection coefficient

Temperature (°C)	ρ_1 (Kg/m ³)	ρ_2 (Kg/m ³)	c_1 (m/s)	c_2 (m/s)	R_{bc}
Room	2219.9	8553	6000	4430	0.4798
200	2219.9	8553	6100	4430	0.47342
300	2219.9	8553	6150	4430	0.47024
400	2219.9	8553	6175	4430	0.46866
500	2219.9	8553	6200	4430	0.46708
600	2219.9	8553	6250	4430	0.46394
700	2219.9	8553	6275	4430	0.46237
800	2219.9	8553	6300	4430	0.46081
900	2219.9	8553	6300	4430	0.46081
1000	2219.9	8553	6325	4430	0.45925
1100	2219.9	8553	6350	4430	0.45769

Table G.1 Sample data sheet for reflection coefficient of brass

Temperature (°C)	ρ_1 (Kg/m ³)	ρ_2 (Kg/m ³)	c_1 (m/s)	c_2 (m/s)	R_{bc}
Room	2219.9	2643	6000	6260	0.10801
200	2219.9	2643	6100	6260	0.09984
300	2219.9	2643	6150	6260	0.0958
400	2219.9	2643	6175	6260	0.09379
500	2219.9	2643	6200	6260	0.09178
600	2219.9	2643	6250	6260	0.0878
700	2219.9	2643	6275	6260	0.08582

Table G.2 Sample data sheet for reflection coefficient of aluminum

Temperature (°C)	ρ_1 (Kg/m ³)	ρ_2 (Kg/m ³)	c_1 (m/s)	c_2 (m/s)	R_{bc}
Room	2219.9	8900	6000	4700	0.51697
200	2219.9	8900	6100	4700	0.51089
300	2219.9	8900	6150	4700	0.50787
400	2219.9	8900	6175	4700	0.50636
500	2219.9	8900	6200	4700	0.50486
600	2219.9	8900	6250	4700	0.50186
700	2219.9	8900	6275	4700	0.50036
800	2219.9	8900	6300	4700	0.49887
900	2219.9	8900	6300	4700	0.49887
1000	2219.9	8900	6325	4700	0.49738
1100	2219.9	8900	6350	4700	0.4959

Table G.3 Sample data sheet for reflection coefficient of copper

Temperature (°C)	ρ_1 (Kg/m ³)	ρ_2 (Kg/m ³)	c_1 (m/s)	c_2 (m/s)	R_{bc}
Room	2219.9	1932	6000	3240	-0.36057
200	2219.9	1932	6100	3240	-0.36774
300	2219.9	1932	6150	3240	-0.37127
400	2219.9	1932	6175	3240	-0.37302
500	2219.9	1932	6200	3240	-0.37475
600	2219.9	1932	6250	3240	-0.3782
700	2219.9	1932	6275	3240	-0.37991
800	2219.9	1932	6300	3240	-0.38161
900	2219.9	1932	6300	3240	-0.38161
1000	2219.9	1932	6325	3240	-0.3833
1100	2219.9	1932	6350	3240	-0.38498

Table G.4 Sample data sheet for reflection coefficient of gold

Temperature (°C)	ρ_1 (Kg/m ³)	ρ_2 (Kg/m ³)	c_1 (m/s)	c_2 (m/s)	R_{bc}
Room	2219.9	1300	6000	2112	-0.65819
200	2219.9	1300	6100	2112	-0.66285
300	2219.9	1300	6150	2112	-0.66513
400	2219.9	1300	6175	2112	-0.66626
500	2219.9	1300	6200	2112	-0.66738
600	2219.9	1300	6250	2112	-0.6696
700	2219.9	1300	6275	2112	-0.6707
800	2219.9	1300	6300	2112	-0.67179
900	2219.9	1300	6300	2112	-0.67179
1000	2219.9	1300	6325	2112	-0.67288
1100	2219.9	1300	6350	2112	-0.67396

Table G.5 Sample data sheet for reflection coefficient of PBI

Temperature (°C)	ρ_1 (Kg/m ³)	ρ_2 (Kg/m ³)	c_1 (m/s)	c_2 (m/s)	R_{bc}
Room	2219.9	2230	6000	5305	-0.0592
200	2219.9	2230	6100	5305	-0.0674
300	2219.9	2230	6150	5305	-0.0715
400	2219.9	2230	6175	5305	-0.0735
500	2219.9	2230	6200	5305	-0.0755
600	2219.9	2230	6250	5305	-0.0795
700	2219.9	2230	6275	5305	-0.0815

Table G.6 Sample data sheet for reflection coefficient of Pyrex

Temperature (°C)	ρ_1 (Kg/m ³)	ρ_2 (Kg/m ³)	c_1 (m/s)	c_2 (m/s)	R_{bc}
Room	2219.9	2180	6000	5585	-0.0449
200	2219.9	2180	6100	5585	-0.0531
300	2219.9	2180	6150	5585	-0.0572
400	2219.9	2180	6175	5585	-0.0592
500	2219.9	2180	6200	5585	-0.0612
600	2219.9	2180	6250	5585	-0.0652
700	2219.9	2180	6275	5585	-0.0672
800	2219.9	2180	6300	5585	-0.0692
900	2219.9	2180	6300	5585	-0.0692
1000	2219.9	2180	6325	5585	-0.0712
1100	2219.9	2180	6350	5585	-0.0731

Table G.7 Sample data sheet for reflection coefficient of silica glass

APPENDIX H-Relative Attenuation Curves

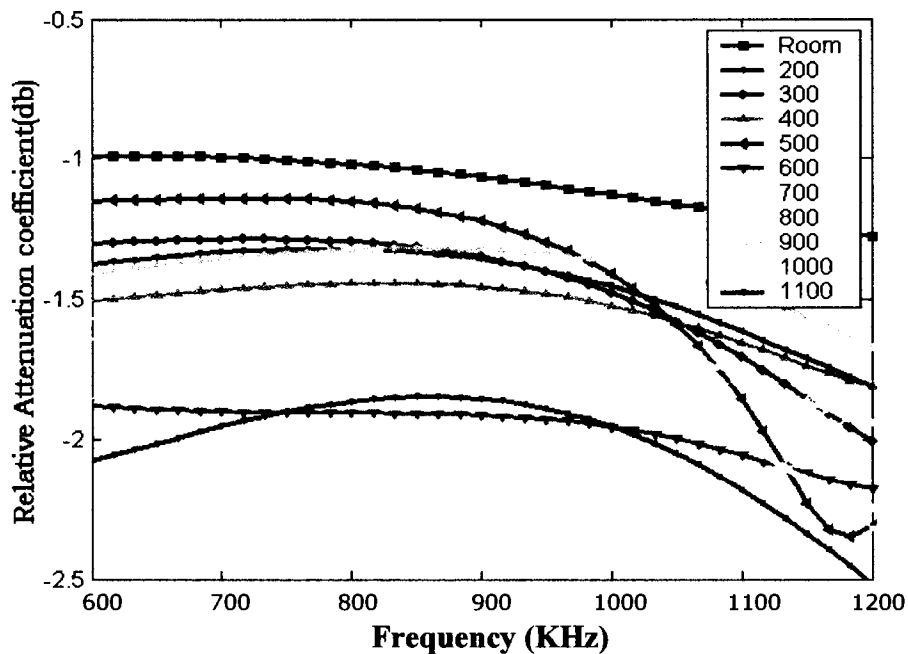


Figure H.1 Relative attenuation coefficient curve for polybenzimidazole from 200-1100°C

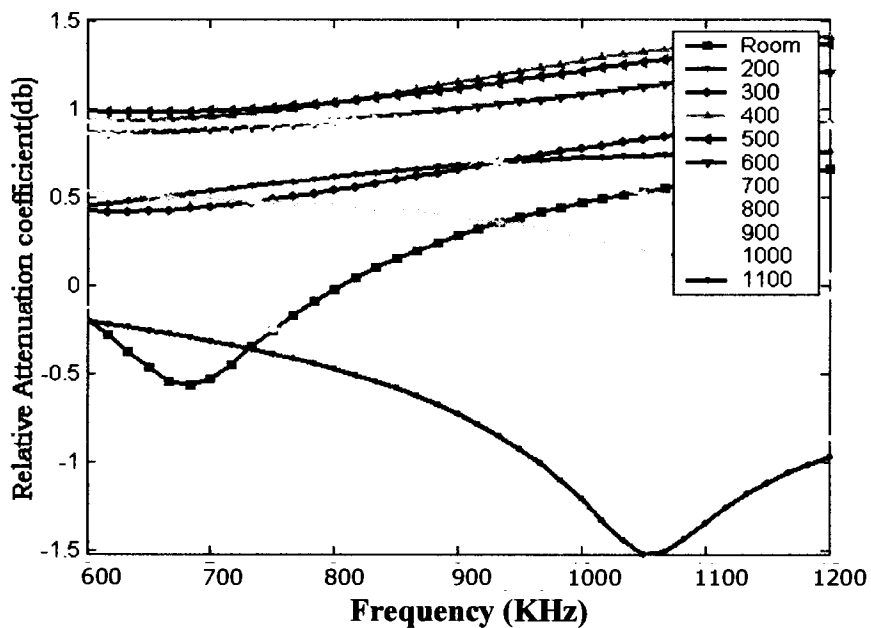


Figure H.2 Relative attenuation coefficient curve for silica glass2 from 200-1100°C

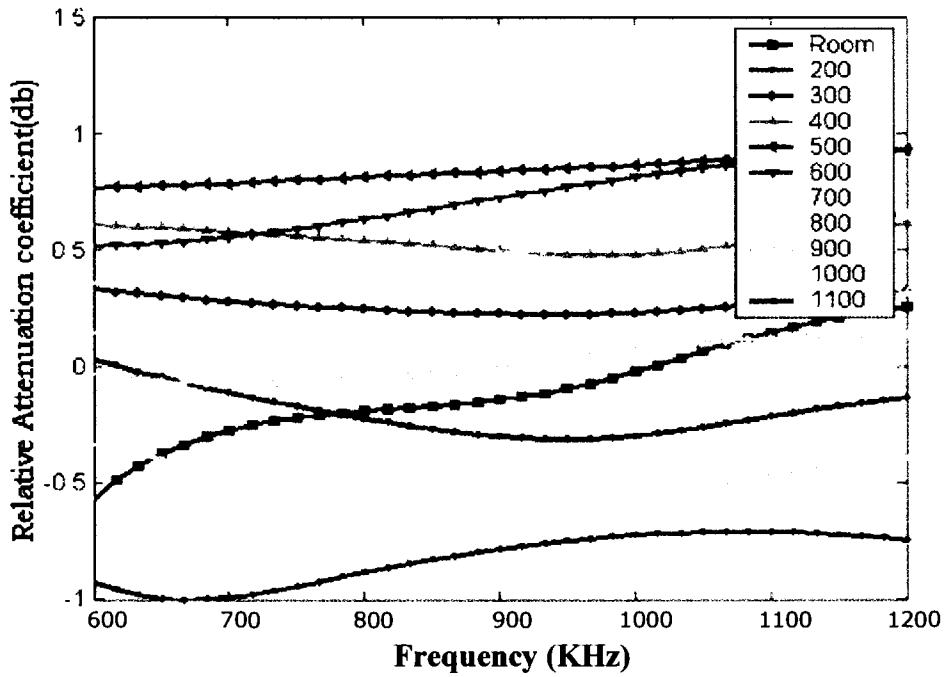


Figure H.3 Relative attenuation coefficient curve for silica glass3 from 200-1100°C

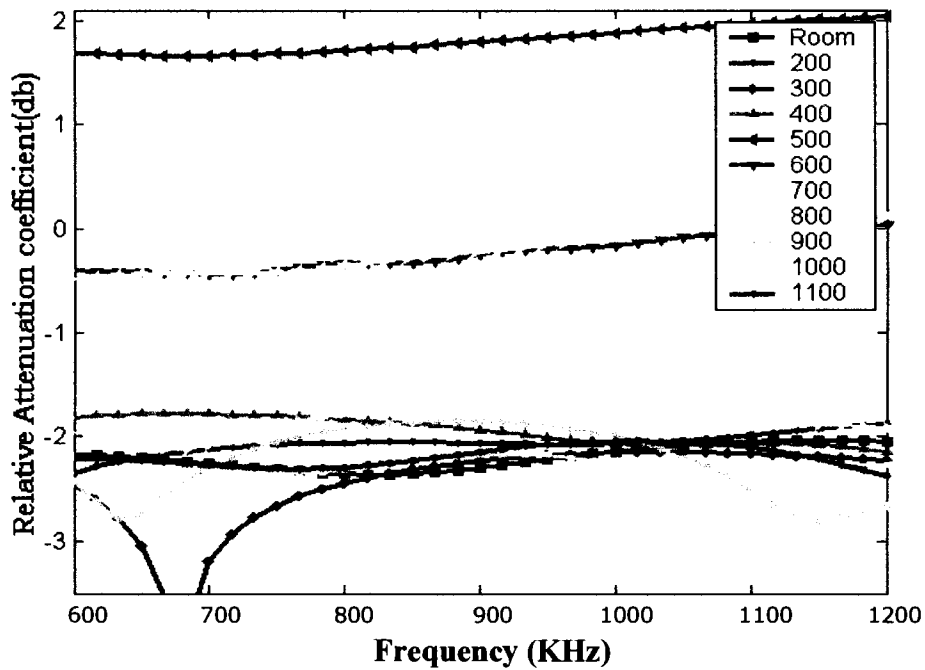


Figure H.4 Relative attenuation coefficient curve for gold 2 from 200-1100°C

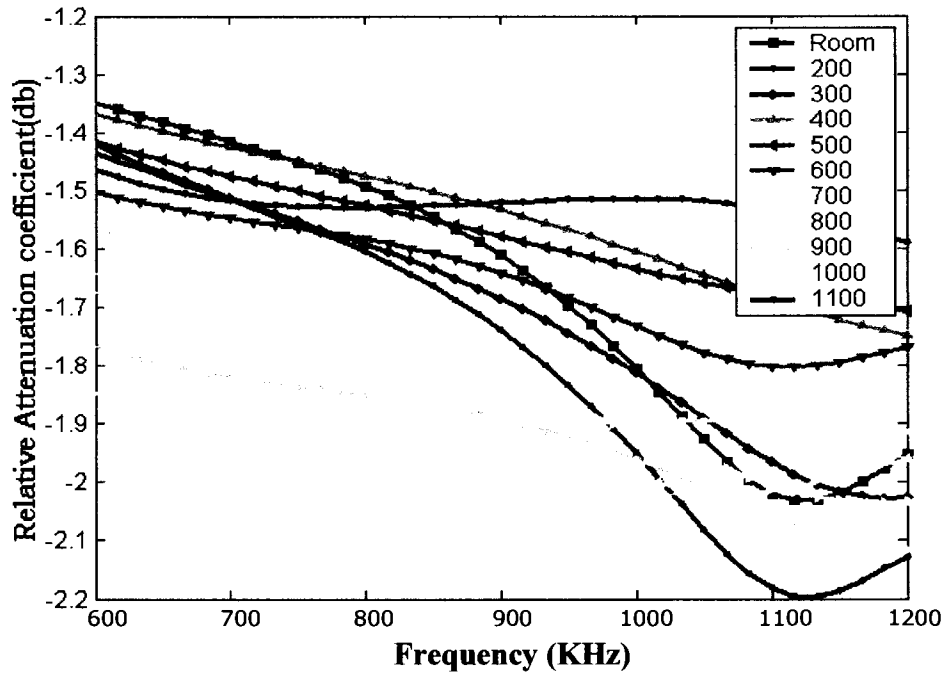


Figure H.5 Relative attenuation coefficient curve for gold 3 from 200-1100°C

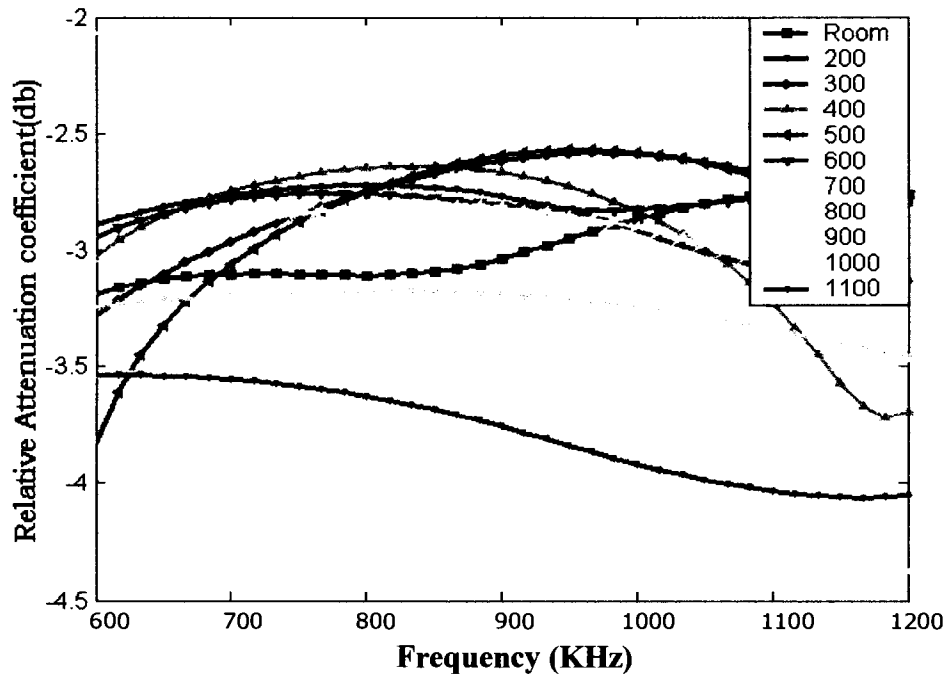


Figure H.6 Relative attenuation coefficient curve for copper from 200-1100°C

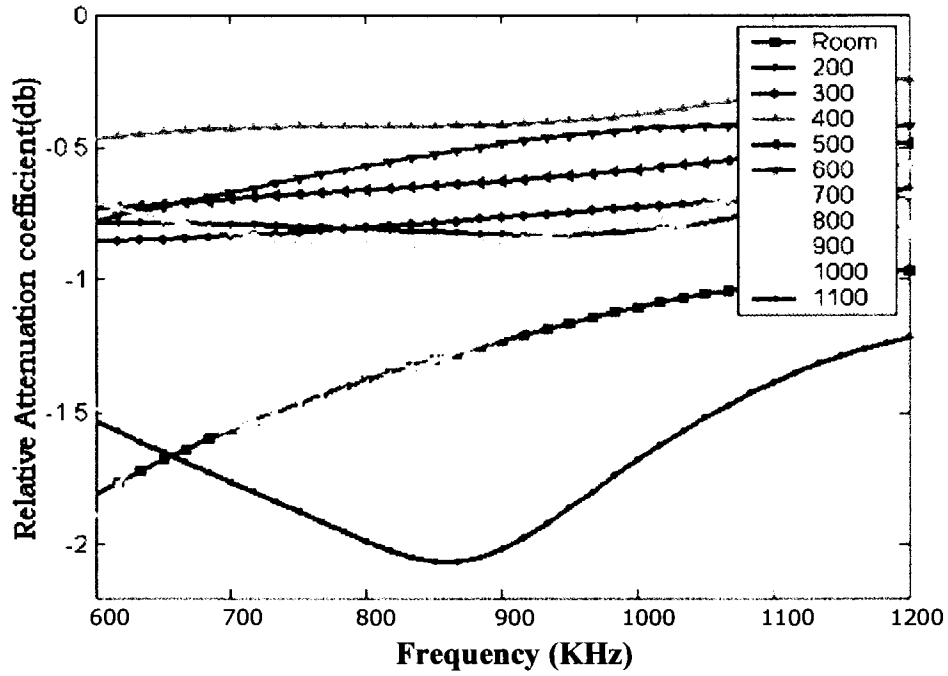


Figure H.7 Relative attenuation coefficient curve for brass at from 200-1100°C

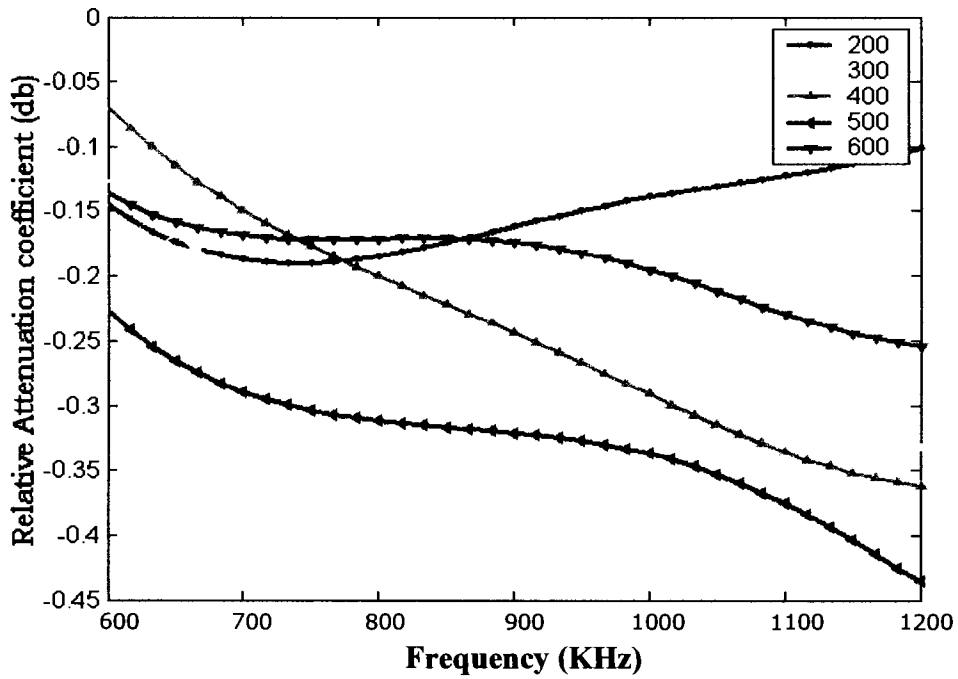


Figure H.8 Relative attenuation coefficient curve for aluminum2 from 200-600°C

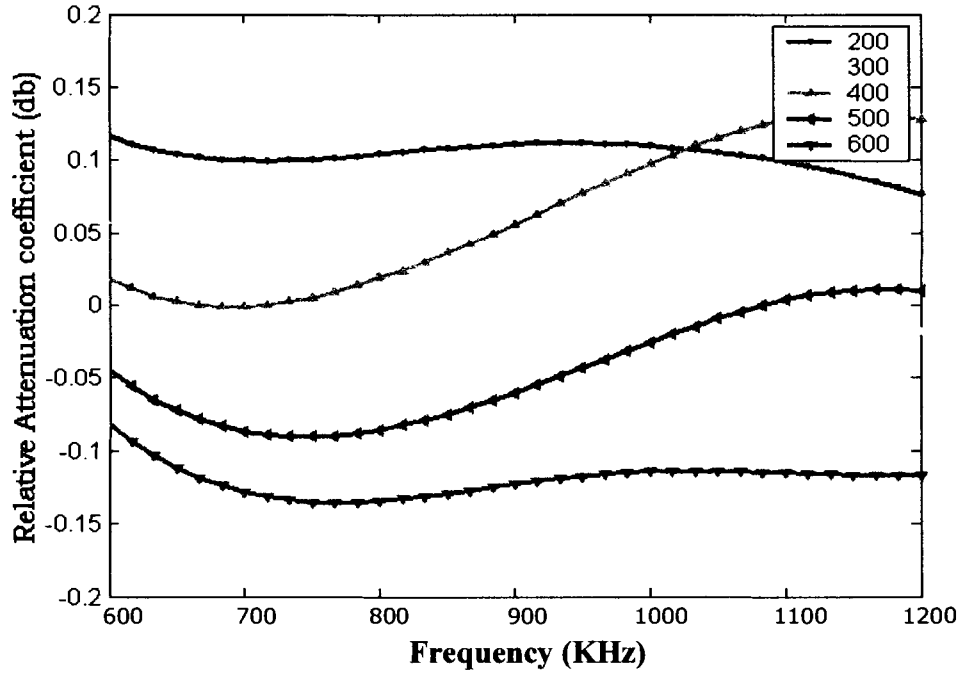


Figure H.9 Relative attenuation coefficient curve for aluminum3 from 200-600°C

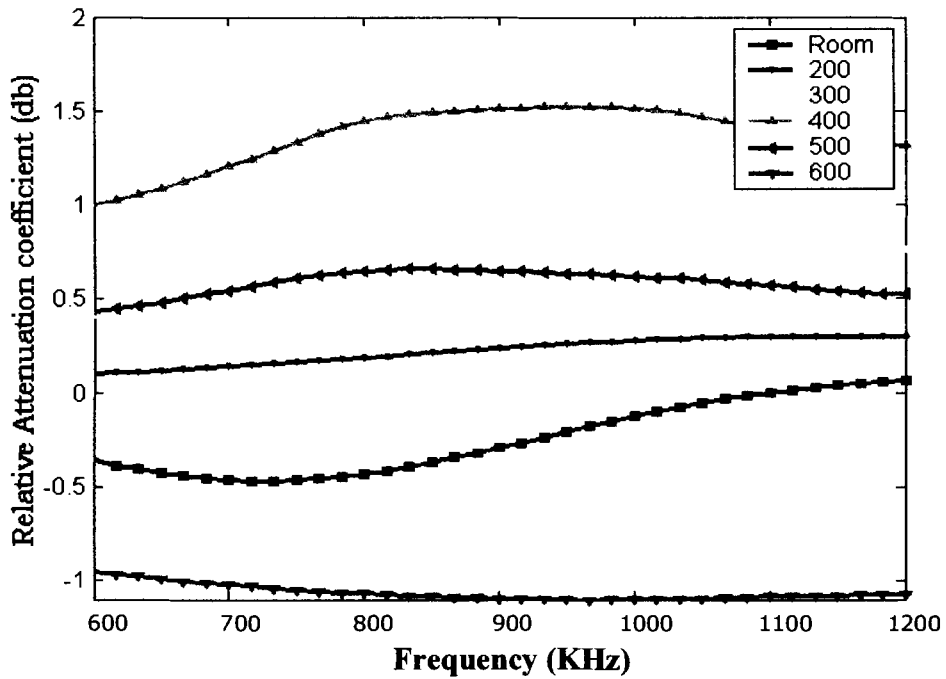


Figure H.10 Relative attenuation coefficient curve for Pyrex from 200-600°C

BIOGRAPHY OF THE AUTHOR

Amala K. Mamilla was born in Narasarao pet, Andhra Pradesh, India on June 30, 1979. She graduated from N.V.R. Junior College, Jonnalagadda, Andhra Pradesh, India in May, 1996. She attended the Mechanical Engineering department at Andhra University in September 1996. She received her Bachelor of Engineering in Mechanical Engineering from Andhra University, Visakhapatnam, India in May, 2000. She then moved to the United States of America to continue her higher education. In January 2002, Amala K. Mamilla began her M.S. program in Mechanical Engineering at The University of Maine.

During her graduate studies at The University of Maine, Amala worked on the research project at the University of Maine. Amala Kishore Mamilla is a candidate for the Master of Science degree in Mechanical Engineering from The University of Maine in August, 2004.